Quantifying groundwater recharge dynamics and unsaturated zone processes in snow-dominated catchments via on-site dissolved gas analysis

O. S. Schilling[1,2,*], A. Parajuli[2,3], C. Tremblay Otis[4], T. U. Müller[1], W. Antolinez Quijano[1,2], Y. Tremblay[1], M. S. Brennwald[5], D. F. Nadeau[2,3], S. Jutras[2,6], R. Kipfer[5,7,8], and R. Therrien[1,2]

[1] Department of Geology and Geological Engineering, Université Laval, Québec, QC, G1V 0A6, Canada.

[2] CentrEau, Quebec Water Research Centre, Université Laval, Québec, QC, G1V 0A6, Canada.

[3] Department of Civil and Water Engineering, Université Laval, Québec, QC, G1V 0A6, Canada.

[4] Centre for Hydrogeology and Geothermics, Université de Neuchâtel, CH-2000 Neuchâtel, Switzerland.

[5] Department of Water Resources and Drinking Water, Swiss Federal Institute of Aquatic Science and Technology (EAWAG), CH-8600 Dübendorf, Switzerland

[6] Department of Wood and Forest Science, Université Laval, Québec, QC, G1V 0A6, Canada.

[7] Institute of Biogeochemistry and Pollutant Dynamics, Swiss Federal Institute of Technology (ETH), CH-8092, Zürich, Switzerland

[8] Institute of Geochemistry and Petrology, Swiss Federal Institute of Technology (ETH), CH-8092 Zürich, Switzerland

* Now at: Centre for Hydrogeology and Geothermics, Université de Neuchâtel, CH-2000 Neuchâtel, Switzerland.

Corresponding author: O. S. Schilling (oliver.schilling@unine.ch)

Highlights:

- On-site measurements of dissolved noble gases allow quantification of groundwater recharge from snowmelt

- Simultaneous measurement of noble gases and O_2, CO_2 and N_2 allows quantification of unsaturated zone processes

- Depletion in N_2 provides evidence for recharging groundwater being the primary source of N_2 for biological N-fixation in boreal forests

Abstract

Snowmelt contributes a significant fraction of groundwater recharge in snow-dominated regions, making its accurate quantification crucial for sustainable water resources management. While several components of the hydrological cycle can be measured directly, catchment-scale recharge can only be quantified indirectly. Stable water isotopes are often used as tracers to estimate snowmelt recharge, even though estimates based on stable water isotopes are biased due to the large variations of δ^2H and $\delta^{18}O$ in snow and the difficulty to measure snowmelt directly. To overcome this gap, a new tracer method based on on-site measurements of dissolved He, ^{40}Ar, ^{84}Kr, N_2, O_2 and CO_2 is presented. The new method was developed alongside classical tracer methods (stable water isotopes, ^{222}Rn, $^3H/^3He$) in a highly instrumented boreal catchment. By revealing (noble gas) recharge temperatures and excess air, dissolved gases allow (i) the contribution of snowmelt to recharge, (ii) the temporal recharge dynamics, and (iii) the primary recharge pathways to be identified. In contrast to stable water isotopes, which produced highly inconsistent snowmelt recharge estimates for the experimental catchment, dissolved gases produced consistent estimates even when the temperature of snowmelt during recharge was not precisely known. As dissolved gases are not controlled by the same processes as stable water isotopes, they are not prone to the same biases and represent a highly complementary tracer method for the quantification of snowmelt recharge dynamics in snow-dominated regions. Furthermore, an observed systematic depletion of N_2 in groundwater provides new evidence for the pathways of biological N-fixation in boreal forest soils.

Key words
groundwater recharge, snowmelt, hydrological tracers, stable water isotopes, noble gases, biological N-fixation

1 Introduction

In many regions around the world, winter hydrological processes such as snowfall, snowmelt, and pore water freeze-thaw strongly affect the hydrological cycle. These regions are characterized by: (1) storage of precipitation in the snowpack in winter, which reduces the amount of surface water (SW) discharge in winter months, and (2) peak SW discharge in the spring, resulting from runoff produced by the concentrated melting of the snowpack (Kinar & Pomeroy, 2015; Kormos et al., 2014; Schilling et al., 2019b). Winter hydrological processes also affect groundwater (GW) recharge, which is defined as the proportion of SW that flows downwards through the topmost layers of Earth's surface and reaches the water table, adding to GW storage (Healy & Scanlon, 2010). Recharge may become largely inhibited in winter due to the retention of precipitation in the snowpack and freezing of the soil. In contrast, recharge from snowmelt during the spring snowmelt period (henceforth called 'snowmelt recharge') can be so large that the relative contribution of snowmelt to annual recharge may even exceed the relative contribution of snowfall to annual precipitation (Earman et al., 2006; Hayashi & Farrow, 2014; Jasechko et al., 2017; Lundberg et al., 2016; Markovich et al., 2019; Meriö et al., 2019; Schilling et al., 2019b; Sturm et al., 2017). A similarly disproportionate relative contribution of snowmelt to SW discharge can also be observed (D. Li et al., 2017; Lundquist, 2018).

In the widespread boreal forests of the northern hemisphere, which make up a significant portion of the snow-dominated regions worldwide, GW represents a crucial drinking water resource. As boreal forests are subject to strong climate change impacts, quantifying recharge

in these systems is particularly important for the sustainable management of water resources (Luke et al., 2007). The effects of winter hydrological processes on the availability of freshwater are so important for the sustainable management of drinking water resources that they are subject of countless ongoing research efforts (Lafrenière & Lamoureux, 2019; Sturm, 2015; Walvoord & Kurylyk, 2016; Young et al., 2020) and are hotly debated (Sturm et al., 2017).

While many components of the hydrological cycle, including streamflow, spring discharge, precipitation and GW levels can be measured with reasonably high precision and accuracy, recharge cannot be measured directly beyond the point scale (Healy & Scanlon, 2010; Scanlon et al., 2002). As recharge most often needs to be quantified over a larger spatial scale, for example at regional- or catchment-scale, it is often estimated indirectly from measurements of hydrological tracers or based on a residual water budget approach (for a comprehensive discussion of available methods see Healy and Scanlon (2010)). The residual water budget approach requires measuring all fluxes in an out of a catchment, and recharge is assumed to be the residual fraction of inflow that does not leave the catchment and contributes to GW storage (Healy & Scanlon, 2010; Scanlon et al., 2002). The accuracy of recharge estimated with that approach is a function of the measurement accuracy of the different water budget components (Risser et al., 2009). For snow-dominated catchments, the uncertainty associated with measurements of evapotranspiration and the water stored and released from snow is typically large, which limits the reliability of the residual water budget approach (Healy & Scanlon, 2010; Scanlon et al., 2002; Smith et al., 2014). Furthermore, the approach requires separation of the SW outflow hydrograph into the direct contribution of precipitation (i.e., runoff) and the contribution of GW (i.e., baseflow), which is also associated with considerable uncertainty (Partington et al., 2012). Due to these existing uncertainties, the residual water budget approach is usually combined with recharge estimations based on hydrological tracers (Cook & Herczeg, 2000; Healy & Scanlon, 2010; Scanlon et al., 2002; Shanafield & Cook, 2014).

There are several natural hydrological tracers applicable to different temporal and spatial scales (Cartwright et al., 2017; Cook & Herczeg, 2000; Kendall & McDonnell, 1998; Purtschert, 2008). However, only a limited number can be used to quantify snowmelt recharge (Kinar & Pomeroy, 2015), with the most common being the stable water isotopes ^{2}H and ^{18}O (commonly expressed in delta notation as δ^2H and δ^{18}O) (Ala-Aho et al., 2018; Ala-Aho et al., 2017a; Ala-Aho et al., 2017b; Beria et al., 2018; DeWalle & Rango, 2008; Hayashi & Farrow, 2014; Jasechko, 2019; McDonnell & Beven, 2014; Schmieder et al., 2016; Sklash & Farvolden, 1979; Tetzlaff et al., 2014). δ^2H and δ^{18}O are affected by many biotic and abiotic processes such as repeated mixing of waters, retention of water in the unsaturated zone, evaporation and plant transpiration, sublimation, interception storage, repeated freeze-thaw, dissolution of organic materials, mineral weathering, and recharge originating at a wide range of elevations (Ala-Aho et al., 2017b; Bansah & Ali, 2017; Beria et al., 2018; Carroll et al., 2018; Cartwright & Morgenstern, 2018; Jasechko, 2019). As a result, the longer the time and distance between precipitation and sampling location, the more δ^2H and δ^{18}O are confounded as tracers of the physical mixing of water from different sources (Beria et al., 2018; Galewsky et al., 2016; Jasechko, 2019; White, 2015). Due to these issues, Kendall and McDonnell (1998) pointed out more than two decades ago that additional tracers are needed for the quantification of the contribution of snowmelt to GW and SW. Electrical conductivity (EC), water temperatures and major ion concentrations are sometimes used as additional tracers, but like δ^2H and δ^{18}O, those tracers are affected by processes other than recharge. Cosmogenic isotopes have also been used to study water storage dynamics of elevated catchments (Visser et al., 2019); however, their suitability has so far only been demonstrated for streamflow and evapotranspiration analyses,

but not for GW recharge. While multiple tracers often get combined into multi-tracer applications (Scanlon et al., 2002), tracer methods more reliable than δ^2H and $\delta^{18}O$ for the quantification of snowmelt recharge still do not exist and therefore have to be developed (Beria et al., 2018; Jasechko, 2019).

Promising alternative tracers for snowmelt recharge are dissolved noble gases (Holocher et al., 2001; Jasechko, 2019; Manning & Caine, 2007; Masbruch et al., 2012; Singleton & Moran, 2010). Concentrations of dissolved noble gases in GW can be used to infer air-saturated water concentrations, estimate the water temperature at the time of recharge (i.e., the noble gas recharge temperature (NGRT)), and to quantify any excess in atmospheric air with respect to the air-water exchange equilibrium concentration (i.e., the excess air (EA)) (Aeschbach-Hertig & Solomon, 2013; Kipfer et al., 2002). Helium concentrations and NGRT have, for example, been used to quantify mountain block recharge into basin aquifers (Manning & Solomon, 2003, 2005) or to quantify recharge from locally infiltrating river water into alluvial aquifers (Beyerle et al., 1999; Mattle et al., 2001; Schilling et al., 2017a). By analyzing dissolved noble gases in subglacial meltwater (Vaikmäe et al., 2001) and underneath artificial recharge ponds (Aeschbach-Hertig & Solomon, 2013; Heilweil et al., 2004), extraordinarily high amounts of EA could be identified. While results from an experimental study by Amalberti et al. (2018) indicated that noble gases within the snowpack may be depleted with respect to the air-water equilibrium, Severinghaus and Battle (2006) have systematically demonstrated that air in the snowpack remains in equilibrium with atmospheric air via molecular diffusion and convection unless the snowpack is 50-100 m thick. As physical processes that convincingly explain noble gas depletion in a snowpack have not been identified and depletion of noble gases in snowmelt has so far not been observed, in snow-dominated headwater catchments with relatively shallow water tables, snowmelt recharge can, therefore, be expected to feature a NGRT close to the melting temperature of snow as well as high EA resulting from a rapid rise of the water table during a concentrated spring recharge pulse. Dissolved noble gases, therefore, bear large potential as tracers for snowmelt recharge. However, concentrations of dissolved noble gases in snowmelt and the potential of noble gases to inform about snowmelt recharge have so far not been systematically evaluated.

Until recently, the simultaneous analysis of multiple gases was only possible through head space or copper tube sampling and subsequent time-consuming and labor-intensive laboratory-based analyses (Aeschbach-Hertig & Solomon, 2013). However, the recently developed gas-equilibrium membrane-inlet portable mass spectrometer (GE-MIMS) has the potential to overcome limitations in spatial and temporal coverage of noble gas analyses, as the GE-MIMS allows on-site and quasi real-time analysis of dissolved noble gases (He, ^{40}Ar, ^{84}Kr) in both water and air, with simultaneous measurement of N_2, CO_2, O_2, H_2 and CH_4 (Brennwald et al., 2016; Mächler et al., 2012; Mächler et al., 2014). By comparing time-series of dissolved ^{40}Ar with O_2 and CO_2, Mächler et al. (2013a) were, for example, able to quantify O_2 consumption and CO_2 production in the hyporheic zone of an alluvial river-aquifer system. Through this, Mächler et al. (2013b) identified EA formation as an important mechanism for the delivery of O_2 to GW. Weber et al. (2018) used dissolved noble gas time-series measured with a GE-MIMS to quantify air-water gas exchange velocities in a shallow lagoon. Tomonaga et al. (2019) employed stationary installations of GE-MIMS to monitor the gas composition in a radioactive waste emplacement experiment. Popp et al. (2020) used dissolved gas time series recorded with a GE-MIMS to quantify the amount of N_2 produced via denitrification in riparian GW. Despite the huge potential and an increasing number of studies that employ the GE-MIMS, so far time-series of dissolved noble gases recorded with a GE-MIMS have not been used to investigate SW-GW dynamics in snow-dominated regions.

The aim of this study was to (i) develop a novel tracer method for the quantification of snowmelt recharge dynamics in a snow-dominated catchment using dissolved gas concentrations measured with a GE-MIMS, and (ii) to compare the snowmelt recharge estimates obtained with dissolved gas concentrations to the existing methods based on measurements of stable water isotopes and a residual water balance approach. The specific goals were (i) to characterize the NGRT and EA signatures of snowmelt recharge in a snow-dominated headwater catchment, (ii) to evaluate the suitability of dissolved gases as complementary tracers alongside stable water isotopes for the quantification of snowmelt-SW-GW dynamics, and (iii) to investigate unsaturated zone processes in boreal soils via simultaneous measurements of noble gases, N_2, O_2 and CO_2. The method was developed in an experimental boreal headwater catchment in Québec, Canada.

2 Materials and Methods
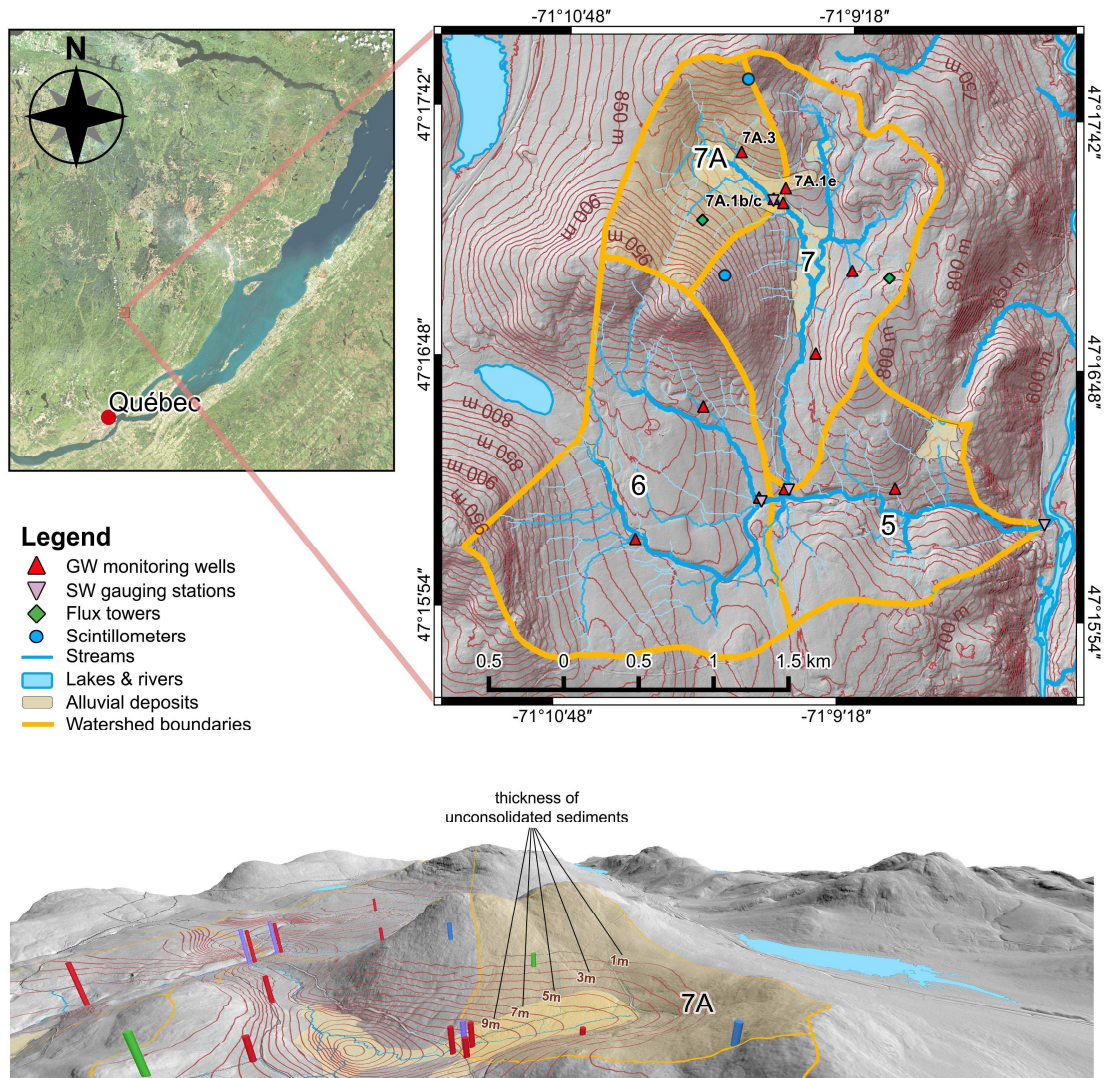
2.1 Study site & monitoring infrastructure

The study was conducted in sub-basin 7A of the well instrumented and well characterized 'Bassin Expérimental du Ruisseau des Eaux-Volées' (BEREV) boreal headwater research catchment, which is situated in the Laurentian Uplands of the Grenville Geological Province on the Canadian Shield (**Figure 1**). The catchment is covered by a balsam fir and white birch forest (Barry et al., 1988; Isabelle et al., 2018; Parajuli et al., 2020a). Being a hanging valley of 1.25 km^2 surface area with an elevation of 775 to 975 m ASL and a topographic slope of approximately 15% on the valley flanks and 10% at the valley bottom, sub-basin 7A strongly resembles the tilted-V benchmark model used widely in numerical SW-GW studies (Kurtz et al., 2017; Maxwell et al., 2014; Panday & Huyakorn, 2004). Owing to its model character, 7A has a long history as a site for hydrological methods development (Barry et al., 1988; Hadiwijaya et al., 2020; Isabelle et al., 2020a; Isabelle et al., 2018; Isabelle et al., 2020b; Lavigne, 2007; Sklash & Farvolden, 1979; Tremblay et al., 2008; Tremblay et al., 2009).

Table 1: Reported average properties of the hydrogeological units at the study site. Composition, horizontal hydraulic conductivity (K_h) and vertical hydraulic conductivity (K_v) were measured by Barry et al. (1988) for soil and by Rochette (1971) for the other units. Porosities for soil are based on saturated water content by Barry et al. (1988), and for the other units on typical values obtained from Anderson et al. (2015) and Gelhar et al. (1992).

Unit name	Soil composition	K_h [m s^{-1}]	K_v [m s^{-1}]	Porosity
soil	Ferro-Humic Podzol	1.4·10^{-5}	1.4·10^{-5}	0.2-0.45
compacted alluvial deposits	59% sand, 30% silt/clay, 11% gravel	3.4·10^{-6}	3.4·10^{-6}	0.25-0.35
unconsolidated glacial deposits	59% sand, 29% gravel, 12% silt/clay	1.4·10^{-5}	1.4·10^{-6}	0.3-0.4
bedrock	Precambrian charnockitic gneiss	2.9·10^{-8}	9.8·10^{-9}	0.02-0.08

The subsurface of 7A consists of very low-permeability Precambrian charnockitic gneiss overlain on 80% of its surface by 1-20 m of unconsolidated deposits of predominantly glacial origin (Légaré-Couture & Parent, 2018; Rochette, 1971; Sklash & Farvolden, 1979; Tremblay Otis, 2018; Tremblay et al., 2008; Tremblay et al., 2009). The unconsolidated glacial deposits are covered by 0-1 m of soil (classification: Ferro-Humic Podzol) (Tremblay et al., 2008; Tremblay et al., 2009). The unconsolidated glacial deposits consist mainly of sand and gravel, forming a variably permeable and anisotropic aquifer (**Table 1**). In the center of 7A and several other sub-basins of the BEREV, an extensive layer of compacted alluvial deposits was identified (a mix of soil, sand and silt; classification: Fragipan and Ortstein) (**Figure 1**), likely formed by a combination of washout and deposition of fine materials as well as compacting by pronounced snowfall, snowmelt and freeze-thaw processes (Barry et al., 1988; Légaré-Couture & Parent, 2018; Rochette, 1971). The alluvial deposits, combined with the anisotropy, create semi-confined conditions.

Figure 1: Top left: Location of the BEREV within Québec, Canada. Top right: Overview of the BEREV, the sub-basins and the monitoring infrastructure. Sub-basin 7A is highlighted by a yellow glow. Elevation contours represent 10 m-intervals. Bottom: 3D view of the BEREV in S-W direction with focus on sub-basin 7A. Contours on the 3D view represent the thickness of the unconsolidated sediments. The vertical dimension in the 3D view is exaggerated by a factor of 2 for better visual presentation. Piezometers, gauging stations, flux towers and scintillometers are indicated by colored pillars. The spatial extent of the alluvial deposits was derived from a combination of on-site observations, the map of Rochette (1971) and the map of Légaré-Couture and Parent (2018). Coordinate system: IGNF:WGS84G. Orthoimage: Esri (2019).

Climatic data for the period 1981-2010 were available from the 'Foret Montmorency RCS' weather station (47°19'22" N, 71°08'54" W) (ECCC, 2013, 2019). The mean annual air temperature observed during that period was 0.5°C, varying between a minimum daily average of -22.1°C in January and a maximum daily average of 20.8°C in July (**Figure 2a**). Mean annual precipitation per calendar year for the same period was 1583 mm, with mean snowfall amounting to 6.6 m and accounting for 40% of the total annual precipitation. In addition, for the period from Oct-2015 to Dec-2018, a flux tower and two scintillometers (see **Figure 1**) provided high-resolution hydrometeorological data for 7A (Isabelle et al., 2020a; Isabelle et al., 2018; Isabelle et al., 2020b; Parajuli et al., 2020b). Mean annual precipitation (per calendar year) recorded during that period was 1444 ± 149 mm/year, with snowfall contributing 40% (Isabelle et al., 2020a). Mean annual evapotranspiration (*ET*) for the same period was 446 ± 33

mm/year and winter water vapor losses accounted for less than 15%, making the contribution of sublimation to the total water balance of 7A relatively minor.

SW discharge out of 7A (Q_{SW}) has been measured continuously since 1995 and averages at 0.04 m^3/s (MELCC, 2019). The discharge peak occurs during the snowmelt period in April-May at an average maximum of 0.15 m^3/s (**Figure 2b**), contributing approximately 50% to the total annual discharge for the catchment. Hydraulic head, EC and water temperature were measured in GW monitoring wells installed in 2017 (**Figure 1**). The location of these wells was constrained by the rugged nature of the terrain and thus they had to be installed near forest roads. The following four GW wells were used in the analysis: A nested piezometer group at the outlet of 7A consisting of one shallow ("shallow GW", well P7A.1c, screen depth: 1-4 m) and one deep well ("deep GW", P7A.1b, screen depth: 9-10.5 m), a piezometer on the lateral boundary of the catchment, representing GW from upstream of the alluvium ("upstream GW", well P7A.1e, screen depth: 3-6 m), and a hillside piezometer located 385 m upstream of the outlet on the north facing slope ("hillslope GW", well P7A.3, screen depth: 4-6 m). The screen depth of the deep GW well was chosen such that it allows sampling of GW and observing hydraulic head between the semi-confining alluvial deposits and the bedrock. For all other GW wells, the screen depth was adapted to cover the range of the local water table fluctuation. Detailed hydrometeorological and hydraulic data are provided in **Supporting Information Table S1**, alongside flux tower-based observations of air pressure, soil temperature at 4 cm depth and snow height.
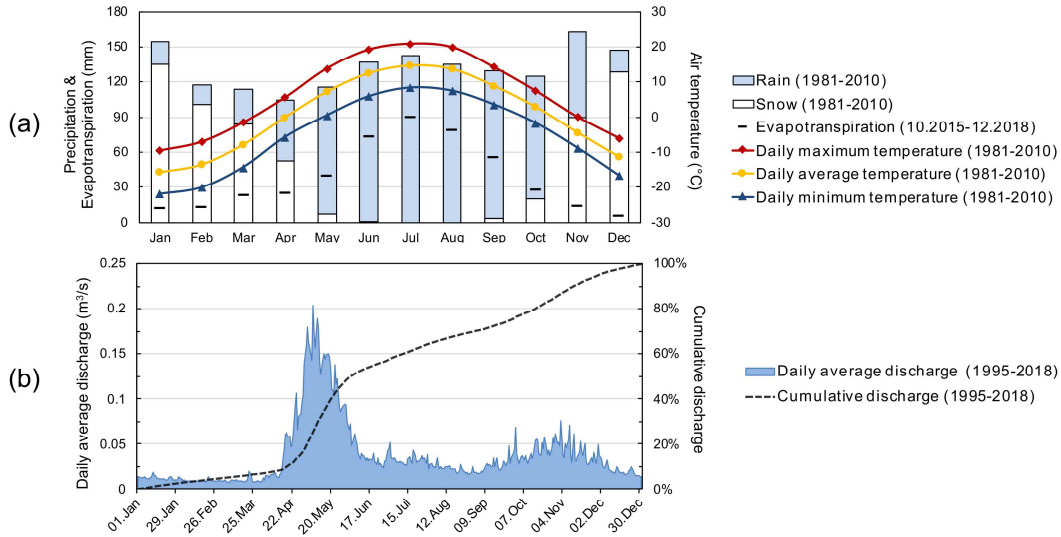
Figure 2: (a) Climate and (b) average daily discharge observed at the study site.

2.2 Residual water budget approach

For headwater catchments such as the one under investigation, SW inflow, GW inflow and SW reservoirs are negligible. Thus, daily net recharge can be estimated with a simple equation based on a residual water budget approach after Healy and Scanlon (2010) and Scanlon et al. (2002), modified for snow-dominated catchments:

$$R = P + \Delta S_{snow} - (Q_{SW} - Q_{baseflow}) - ET \qquad (1)$$

where R is net recharge, P is liquid precipitation, Q_{SW} is SW outflow, $Q_{baseflow}$ is the component of SW outflow contributed by GW storage, ET is the sum of evaporation, plant transpiration and sublimation, and ΔS_{snow} is the change in the snow reservoir attributable to melting (i.e., snowmelt). All variables in **Equation 1** are expressed as an equivalent height of water. To obtain an equivalent height of water for outflow terms (i.e., for Q), volumetric flow rates were divided by the catchment area and aggregated to daily sums. When the average daily air temperature was below 1°C, precipitation was assumed to be solid and P considered to be zero on that day. Daily ΔS_{snow} was quantified from the daily decrease in snow depth (d_{snow}) attributable to melting (i.e., for daily average air temperatures $\geq$ 2°C). d_{snow} was measured daily near the 7A flux tower (Parajuli et al., 2020a). The different ET components were not measured separately. However, research by Isabelle et al. (2020a) and Hadiwijaya et al. (2020) and the stable water isotope analyses of this study revealed that sublimation and plant transpiration were negligible in winter and during the snowmelt period, therefore, loss of snow to sublimation was assumed negligible for the calculation of ΔS_{snow}. To calculate ΔS_{snow}, d_{snow} was transformed into snow water equivalent according to Sturm et al. (2010) using the average snow density (ρ_{snow}) observed underneath the flux tower (i.e., 0.335 g/cm^3; Parajuli et al. (2020a)). $Q_{baseflow}$ was estimated with the Lyne and Hollick (1979) recursive digital filter using the recommended filter value for small catchments (i.e., 0.9) (Eckhardt, 2005; Fuka et al., 2018; L. Li et al., 2014; Nathan & McMahon, 1990; Partington et al., 2012).

2.3 Classical hydrological tracers

Sampling and analysis of the classical hydrological tracers stable water isotopes, ^{222}Rn and ^{3}H/^{3}He was conducted following standard protocols. Details on sampling methodology, location, storage and analysis are provided in **Supporting Information Text S1**.

2.4 On-site dissolved gas analysis

2.4.1 On-site measurement of dissolved gases with the GE-MIMS

The GE-MIMS allows simultaneous measurement of a wide range of gases in air and dissolved in water directly on-site, in near-real-time (one sample every 10 minutes) and with an analytical uncertainty of 1-3% (Brennwald et al., 2016). For operation at the air-water-equilibrium, the GE-MIMS can be calibrated on-site with ambient air. However, in order to reach the maximum precision possible with the GE-MIMS, the instantaneous atmospheric pressure must be known to quantify the amount of ambient air used for calibration. For the dissolved gas analysis, SW and GW were pumped through a 3M G542 Liqui-Cel MiniModule flow-through membrane contactor at approximately 2 L/min using a peristaltic pump. The gases were subsequently transferred to the mass spectrometer via a 10 m rugged stainless-steel capillary that simultaneously prevents leakage of gases while reducing the pressure of the sample gas from approximately atmospheric pressure to the pressure required for the high vacuum. Due to extreme winter conditions, the GE-MIMS was housed in a heated mobile laboratory mounted on a snowmobile trailer (Schilling et al., 2018). The sampling frequency was adapted to the system (i.e., higher frequency before, during and after snowmelt) and to the accessibility and weather conditions of the site. From Dec-2017 until May-2018, GW could only be sampled from well 7A.1b (deep GW) as all other wells were clogged by ice. Concentrations of He, ^{40}Ar, ^{84}Kr, N_2, O_2, and CO_2 were obtained from the mass spectrometer readings following the procedure described by Brennwald et al. (2016), using the atmospheric pressure measurements from the 7A flux tower (see **Fig. 1**) for calibration gas quantification.

2.4.2 Quantification of noble gas recharge temperature and excess air

The equilibrium concentration of a chemically inert atmospheric gas i in water can be expressed by Henry's Law of gas exchange (Aeschbach-Hertig & Solomon, 2013; Kipfer et al., 2002):

$$C_{i,R}^{ASW} = \frac{x_i(P_R - p_{H_2O})}{K_i(T_R, S_R)} \tag{2}$$

where $C_{i,R}^{ASW}$ (cm_{STP}^3/g_{H_2O}) is the equilibrium concentration in air-saturated water (ASW), x_i (-) is the mole fraction in dry air and $K_i(\frac{hPa}{cm_{STP}^3/g_{H_2O}})$ is the Henry coefficient of gas i, P_R (hPa) is the total atmospheric pressure, p_{H_2O} (hPa) is the saturation water vapor pressure, T_R (°C) is the water temperature at the time of recharge (i.e., the NGRT), and S_R (g/kg) is the water salinity at the time of recharge (commonly assumed to be zero in freshly infiltrated water).

As a result of water table fluctuations, air bubble entrapment and the related air bubble dissolution during recharge, GW is typically oversaturated in inert atmospheric gases (Aeschbach-Hertig et al., 1999, 2000; Aeschbach-Hertig & Solomon, 2013; Kipfer et al., 2002). The recharge concentration $C_{i,R}$ (cm_{STP}^3/g_{H_2O}) of gas i can, therefore, be expressed by:

$$C_{i,R} = C_{i,R}^{ASW} + C_{i,R}^{EA} \tag{3}$$

where $C_{i,R}^{EA}$ (cm_{STP}^3/g_{H_2O}) is the excess air component. A physical description of the formation of EA is given by the closed equilibrium (CE) model, which postulates a local partitioning equilibrium between the entrapped air/gas phase and the surrounding GW (Aeschbach-Hertig et al., 2008; Aeschbach-Hertig et al., 2000; Kipfer et al., 2002):

$$C_{i,R}^{EA} = C_{i,R}^{ASW} \frac{(1-F)A_e H_i}{1 + F A_e H_i} \tag{4}$$

where H_i (-) is the dimensionless Henry coefficient of gas i, F (-) is the fractionation coefficient and A_e (cm_{STP}^3/g_{H_2O}) the initial amount of entrapped air. If only part of the initially entrapped air in a water parcel is dissolved, then $0 < F \leq 1$. If all A_e is dissolved, then F equals 0, A_e equals EA and **Equation 4** becomes equivalent to the model for unfractionated excess air (UA) (Aeschbach-Hertig & Solomon, 2013; Heaton & Vogel, 1981; Kipfer et al., 2002).

If P_R and S_R and the concentration of at least three noble gases are known, then T_R, A_e and F can be identified inversely using one of the available noble gas algorithms (Aeschbach-Hertig & Solomon, 2013; Brennwald, 2014; Jung & Aeschbach-Hertig, 2018). However, the GE-MIMS is only capable of measuring He and ^{40}Ar at sufficient accuracy for the small concentrations typically encountered in young GW. With only two noble gases available, the equation system is underdetermined and a suitable proxy for F must be identified. As demonstrated by Holocher et al. (2002) and Peeters et al. (2002), if the ratios of Ne/Ar and ^{4}He/^{20}Ne in GW are close to the ASW equilibrium ratio for the expected recharge conditions, EA is either unfractionated or so small that the CE model converges into the UA model. If the UA model applies, F can be set to 0, EA equals A_e, and T_R and A_e can be inversely identified with He and ^{40}Ar, provided that significant local subsurface sources for He and ^{40}Ar can be ruled out. Significant local subsurface sources of He can be ruled out if the He/^{40}Ar ratio does not indicate production and the GW is young (i.e., ^{3}H > 5 TU) (Aeschbach-Hertig & Solomon, 2013; Kipfer et al., 2002; Mayer et al., 2014). Significant radiogenic production of ^{40}Ar is

commonly only observed for GW with residence times on the order of 10^5 years or more and can be ruled out if the $^{40}Ar/^{36}Ar$ ratio in GW is not significantly larger than the atmospheric ratio (i.e., 298.56; Böhlke (2014)) (Aeschbach-Hertig & Solomon, 2013; Kipfer et al., 2002)).

P_R and S_R were available in this study via atmospheric pressure observations from the 7A flux tower and EC observations from the deep GW. Noble gas isotopic ratios of the deep GW were available from high-resolution noble gas isotope measurements made for the $^3H/^3He$ residence time analysis (see **Supporting Information Text S1** for details on sampling and analysis). As reported in further detail in **section 3.5**, at the studied site significant local subsurface sources for He and ^{40}Ar do not exist and the UA model applies. Therefore, F could be set to 0 and T_R and A_e were inversely identified with concentrations of He and ^{40}Ar using the noble gas algorithm *noblefit* (Brennwald, 2014).

### 2.4.3 Analysis of biogeochemical subsurface activity based on dissolved N_2, O_2 and CO_2

When measured individually, concentrations of N_2, CO_2 and O_2 dissolved in GW and SW are difficult to interpret due to the diverse biotic and abiotic processes that can alter their concentration after recharge (Brennwald et al., 2016; Kipfer et al., 2002). Besides microbial respiration and denitrification, which are ubiquitous in soils, biological fixation of atmospheric N_2 within boreal soils is thought to play a key role in the N-cycle of boreal systems (DeLuca et al., 2002; DeLuca et al., 2008; Kuypers et al., 2018; Puri et al., 2020; Rolston, 2005; Sponseller et al., 2016). If N_2, CO_2 and O_2 are measured in parallel to noble gases, the initial amounts of N_2, CO_2 and O_2 present in a water parcel during the moment of recharge can be quantified, which in turn allows biogeochemical sources and sinks for N_2, CO_2 and O_2 to be identified (Brennwald et al., 2016; Mächler et al., 2013a; Mächler et al., 2013b; Popp et al., 2020). For a quantitative interpretation of CO_2, the GE-MIMS would need to be calibrated against a standard gas with known CO_2 concentration, as CO_2 in ambient air exhibits large variability and low partial pressure. However, if partial pressures of CO_2 are orders of magnitudes higher in GW compared to ambient air, the raw CO_2 ion currents recorded by the mass spectrometer (in ampere) can be interpreted qualitatively without calibration relative to a gas standard (Mächler et al., 2013a).

3 Results

3.1 Hydraulic and meteorological data
The hydraulic and meteorological parameters observed between 01-Nov-2017 and 31-Dec-2018 are illustrated in **Figure 3** (the full dataset is available as **Supporting Information Table S1**). From the start of the winter season on 01-Nov-2017 until the onset of the spring snowmelt period on 22-Apr-2018, the average daily air temperature remained below 0°C. Soil temperature remained around 0°C throughout winter. Precipitation was evenly distributed throughout the entire study period, with winter precipitation from 01-Nov-2017 until 22-Apr-2018 amounting to 642 mm. Except for two significant rain-on-snow events on 12-Jan-2018 and 22-Feb-2018, which are visible as spikes in the SW discharge and hydraulic heads, precipitation in winter fell as snow and SW discharge remained minimal. The spring snowmelt period lasted from 22-Apr-2018 until 31-May-2018. During this period, SW discharge rose dramatically while the in-stream EC dropped to virtually 0 µS/cm – a clear sign that stream water during the snowmelt period was entirely made up of snowmelt and precipitation. Immediately after the snowmelt period, in-stream EC started to rise. By mid-summer, it had reached levels higher than the pre-snowmelt levels, indicating that the SW after the snowmelt period predominantly derived from exfiltrating GW. In-stream EC was higher post- than pre-snowmelt, which may have resulted from a larger post-snowmelt contribution of GW to SW,

or from older and more minerally-enriched GW exfiltrating into the stream post-snowmelt compared to pre-snowmelt. Both scenarios are compatible with the large seasonal shifts in hydraulic gradients observed at the outlet of 7A.
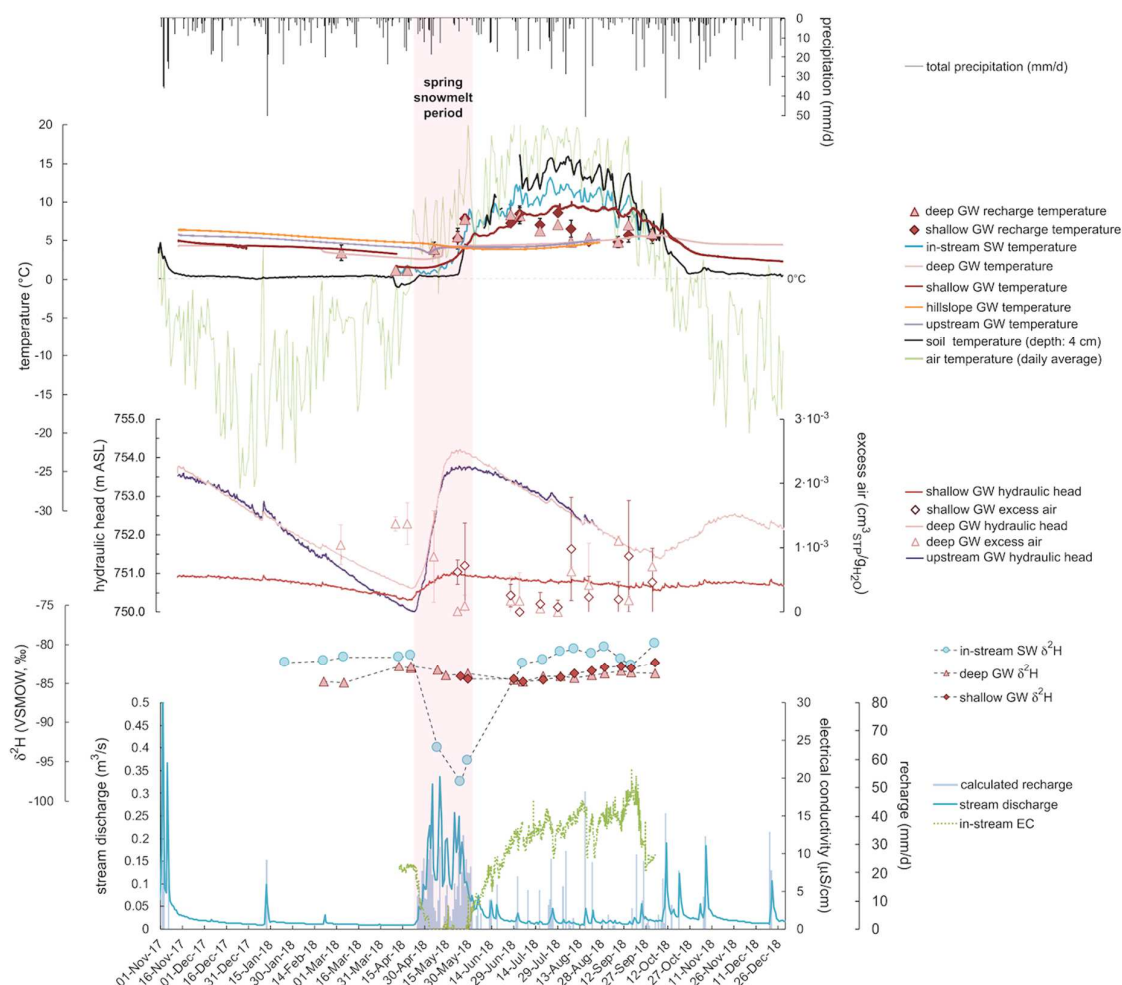
Figure 3: Illustration of the recorded hydraulic and meteorological data together with δ^2H, NGRT and EA. The daily variation in NGRT and EA is illustrated by error bars representing 2-σ intervals. Error bars for δ^2H, which are smaller than the used symbols, represent 2-σ measurement uncertainty intervals. Daily net recharge estimated from closing the water balance is illustrated alongside SW discharge and in-stream EC.

Despite the fact that the shallow and upstream GW wells could not be sampled until spring because water in the top 0.5 m was frozen, hydraulic head could be recorded in all wells as they were sealed off either by ice (shallow GW and upstream GW) or by a sub-frost packer (deep GW). In the upstream and the deep GW, the hydraulic head declined linearly by 4 m during winter. The water table (i.e., hydraulic head in the shallow GW) declined by 0.5 m during the same period. The recorded hydraulic head profiles at the outlet exhibit a clear upward gradient from deep to shallow GW, as the hydraulic head of the semi-confined deep GW was always higher than that of the shallow GW. The semi-confined deep GW of the deep GW well was artesian throughout the entire study period. The fact that not only the deep but also the shallow GW reacted immediately to the two rain-on-snow events indicates that also the shallow GW is partially confined, allowing pressure to propagate rapidly through both deep and shallow GW.

During the short spring snowmelt period (see highlighted area in **Fig. 3**), hydraulic heads rose dramatically, increasing by more than 4 m in the upstream GW and the deep GW and 0.6 m in the shallow GW. Due to the strong upward gradient from deep to shallow GW at the outlet of 7A, recharge must have occurred in the upstream parts of 7A. The shape of the hydraulic head variations in the upstream GW and the hillslope GW (hillslope GW not shown in **Figure 3**, see **Supporting Information Table S1**) correspond to that in the deep GW. However, the variations in the hillslope GW were larger and the depth to GW in the hillslope GW well varied between 0.9 and 5.3 m (see **Supporting Information Table S1**).

As can be expected for a GW sampling depth of 10 m, the temperature of deep GW did not change significantly in response to recharge and remained close to the average annual mean of 5.3°C, indicating long flow paths along which the GW temperature approaches the mean shallow GW temperature. The temperature of hillslope GW and upstream GW followed a similar pattern as the deep GW. The temperature of shallow GW, on the other hand, reacted more strongly than the deep, upstream and hillslope GW, and reflects the patterns of SW and air temperatures during spring and summer. Given the strong upward gradient in GW at the outlet, the temperature rise of the shallow GW is likely the result of conductive heat transfer from the atmosphere through the soil rather than of local recharge or upwelling of deep GW.

Daily recharge estimated using the residual water budget approach is illustrated at the bottom of **Figure 3**. Recharge peaks match well with the observed variations in hydraulic head and SW discharge.

3.2 Stable water isotopes

In **Figure 3**, the temporal evolution of δ^2H for in-stream SW, shallow GW and deep GW is shown alongside hydraulic and meteorological data ($\delta^{18}O$ is not shown, as the temporal evolution of $\delta^{18}O$ reflects the same pattern). Measured δ^2H and $\delta^{18}O$ for rain, snowfall, the snowpack shortly after the onset of the snowmelt in early May, in-stream SW, shallow GW and deep GW are illustrated in **Figure 4**. Samples that could not be clearly associated with snowfall or rain based on the sampling information were discarded. The full δ^2H and $\delta^{18}O$ dataset is provided in **Supporting Information Table S2**.
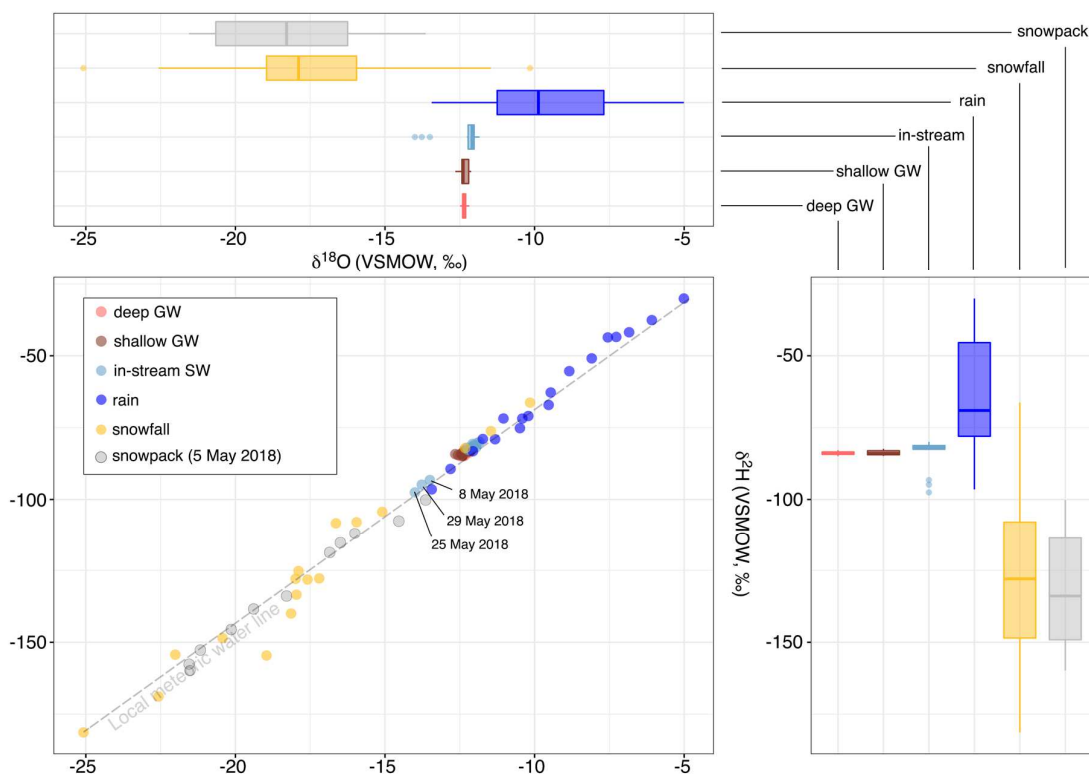
Figure 4: Measured δ^2H versus measured $\delta^{18}O$, with respective boxplots. Local meteoric water line (LMWL): $\delta^2H = (1.654+\delta^{18}O)/0.1261$.

As expected, snowfall can be clearly distinguished from rain due to its strong depletion of heavy isotopes compared to rain (mean difference of -62‰ in δ^2H, -8‰ in $\delta^{18}O$). As none of the samples deviate systematically from the local meteoric water line (LMWL), a significant influence of evapotranspiration or sublimation on SW and GW in 7A can be ruled out. The snowpack during the onset of the spring snowmelt period was similar to snowfall, albeit slightly more depleted in heavy isotopes (mean difference of -5.5‰ in δ^2H, -0.7‰ in $\delta^{18}O$). A significant melt-out effect (i.e., a loss of lighter isotopes due to partial melting prior to the spring snowmelt period) could therefore not be observed. This is consistent with the observed air temperatures and SW discharge during winter (**Figure 3**), which also suggests that no significant melting took place prior to the spring snowmelt period.

Neither shallow nor deep GW showed significant variation in isotopic composition throughout the entire sampling period, averaging at -84‰ in δ^2H and -12.4‰ in $\delta^{18}O$, respectively (**Figures 3 and 4**). The fact that δ^2H and $\delta^{18}O$ in GW remained stable reveals that the water from different recharge periods is homogenized before arriving at the outlet of 7A. A substantial unsaturated zone, in which waters from different recharge events are retained and mixed prior to reaching the GW, could explain this behavior. Throughout most of the sampling period, SW was slightly more enriched in heavy isotopes compared to GW, but nevertheless very close to GW (mean -84‰ in δ^2H and -12.4‰ in $\delta^{18}O$). The spring snowmelt period is the only time when the isotopic signature of SW was significantly more depleted than GW (mean -95‰ in δ^2H and -13.8‰ in $\delta^{18}O$) (**Figures 3 and 4**). As a significant amount of rain was recorded during the spring snowmelt period (**Figure 3**), in-stream δ^2H and $\delta^{18}O$ were likely enriched during that period and not reflective of pure snowmelt.

3.3 ^{222}Rn and ^{3}H/^{3}He

With an average of 9.2 kBq/m^3, the ^{222}Rn activity concentration in the shallow and the deep GW wells did not vary significantly considering the 2-σ analytical uncertainty interval, indicating that ^{222}Rn in both shallow and deep GW was in secular equilibrium and the GW residence time $\geq$ 14 days throughout the entire sampling period (individual measurements are provided as **Supporting Information Table S2**). Local recharge at the outlet of 7A can therefore be ruled out. The average in-stream ^{222}Rn activity concentration at the outlet of 7A before the spring snowmelt period was 0.4 kBq/m^3, revealing a significant contribution of GW to the stream. During the snowmelt period, the in-stream ^{222}Rn activity concentration dropped to virtually zero (< 0.1 kBq/m^3), indicating a strong reduction of the relative contribution of GW to SW. Due to the strong potential for degassing of ^{222}Rn to the atmosphere once GW enters the stream at the study site, the contribution of GW to SW could not be reliably quantified based on ^{222}Rn.

Based on a copper tube sample taken in the deep GW well on 29-May-2018, a high-resolution noble gas isotope analysis revealed that the ^{3}H concentration and the ^{3}He/^{4}He ratio in the deep GW at the outlet of 7A were 9.6 $\pm$ 0.4 TU and (1.42 $\pm$ 0.01)$\cdot10^{-6}$, respectively (detailed noble gas isotope data are provided in **Supporting Information Table S2**). The corresponding ^{3}H/^{3}He-residence time is 3.9 $\pm$ 0.9 years, indicating a significant lag between the time of recharge and the arrival of GW at the outlet of 7A.

3.4 Dissolved gases measured on-site with the GE-MIMS

Concentrations of He, ^{84}Kr and N$_2$ observed in the deep GW are compared to concentrations of ^{40}Ar in **Figure 5**. Concentrations of O$_2$ and ampere readings of CO$_2$ observed in the deep GW are compared to one another and to concentrations of ^{40}Ar in **Figure 6**. The ASW equilibrium for the average P$_R$ (i.e., 911 hPa) and average S$_R$ (i.e., 0 g/kg) observed at the study site are indicated by black dashed lines in **Figures 5 and 6**. To account for the strong dependency of He on P$_R$, a 2-σ confidence interval for ASW, as given by the standard deviation of the atmospheric pressure observed at the studied site (i.e., $\pm$10 hPa), is indicated by grey dashed lines in **Figure 5a**. Hypothetical additions of unfractionated EA to the ASW equilibrium are indicated by finely dotted grey lines for 0°C, 5°C, 10°C, 15°C and 20°C. As shallow GW exhibited concentrations and patterns similar to the deep GW, only deep GW measurements are illustrated in **Figures 5 and 6** (individual dissolved gas measurements are provided in **Supporting Information Table S2**).

For ^{40}Ar, He and N$_2$, clear seasonal trends could be observed (**Figure 5a and 5b**): GW sampled in April immediately before the onset of snowmelt exhibited the largest concentrations of He, N$_2$ and ^{40}Ar, whereas GW sampled during mid-summer in late June/early July exhibited the lowest concentrations. ^{40}Ar, He and N$_2$ varied systematically between these two extremes. Due to the large measurement uncertainty of ^{84}Kr (**Figure 5c**), a clear seasonal trend could not be observed, and a reliable interpretation of ^{84}Kr is not possible.

In almost all samples, N$_2$ concentrations were significantly depleted with respect to ASW (**Figure 5b**). This systematic and consistent depletion suggests the presence of an N$_2$ sink in the subsurface. In contrast, the slight depletions in He concentrations are statistically insignificant given the overall analytical uncertainties. Statistically significant deviances in He (depletion) and ^{84}Kr (enrichment) concentrations with respect to ASW are only observed in samples obtained on 24-May-18 and 29-Jun-18 (**Figure 5a and 5c**). This elemental fractionation seems to indicate some kind of degassing process during sampling. These samples are therefore interpreted as outliers and not considered for further analyses.
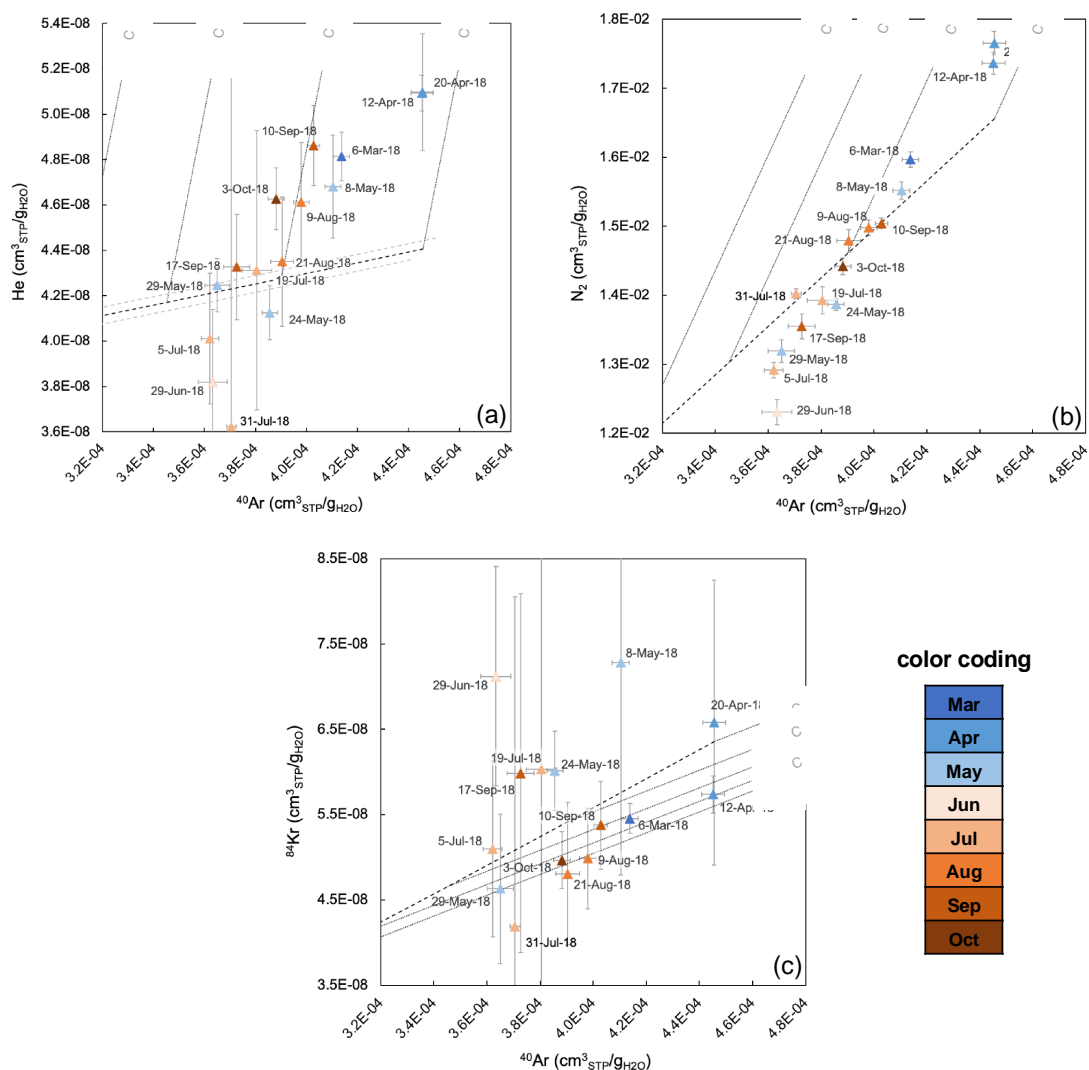
Figure 5: Bi-species plots of average daily concentrations of dissolved inert gases observed in the deep GW well (P7A.1b). Markers are color coded by sampling month and error bars represent 2-σ uncertainty intervals. The dashed black line indicates ASW between 0°C and 30°C for the average atmospheric pressure of the studied site (i.e., 911 hPa). The dashed grey lines represent the 2-σ uncertainty interval for ASW as given by the standard deviation of the average atmospheric pressure at the studied site (i.e., 10 hPa). The ASW uncertainty interval is only indicated for (a) as only He is significantly affected by this atmospheric pressure variation. Grey lines represent hypothetical additions of unfractionated excess air to ASW at different temperatures. Within the experimental errors (which are considerably larger for ^{84}Kr) and in line with the general geochemical analyses, the noble gases He, ^{40}Ar, ^{84}Kr that were observed in the field with the portable GE-MIMS system are only of atmospheric origin and can be interpreted as mixtures of ASW and EA.

The seasonal behavior observed for He, N_2 and ^{40}Ar could also be observed for O_2. GW was consistently depleted in O_2 with respect to ASW throughout the entire sampling period (**Figure 6a**), with depletion being strongest at the end of winter immediately before snowmelt and least pronounced during summer. Despite a significant depletion, the smallest observed O_2 concentration was still 7.7 mg/L (20-Apr-2018), thus, indicating that the GW remained in an oxic state throughout the entire observation period. CO_2 also exhibited a seasonal trend with respect to ^{40}Ar (**Figures 6b**), albeit in the opposite direction of O_2 (**Figure 6c**): The largest amount of dissolved CO_2 (i.e., strongest ion current) was observed in winter when the depletion in O_2 was largest, while the smallest amount of CO_2 was observed in late summer to autumn, when the depletion in O_2 was least pronounced.
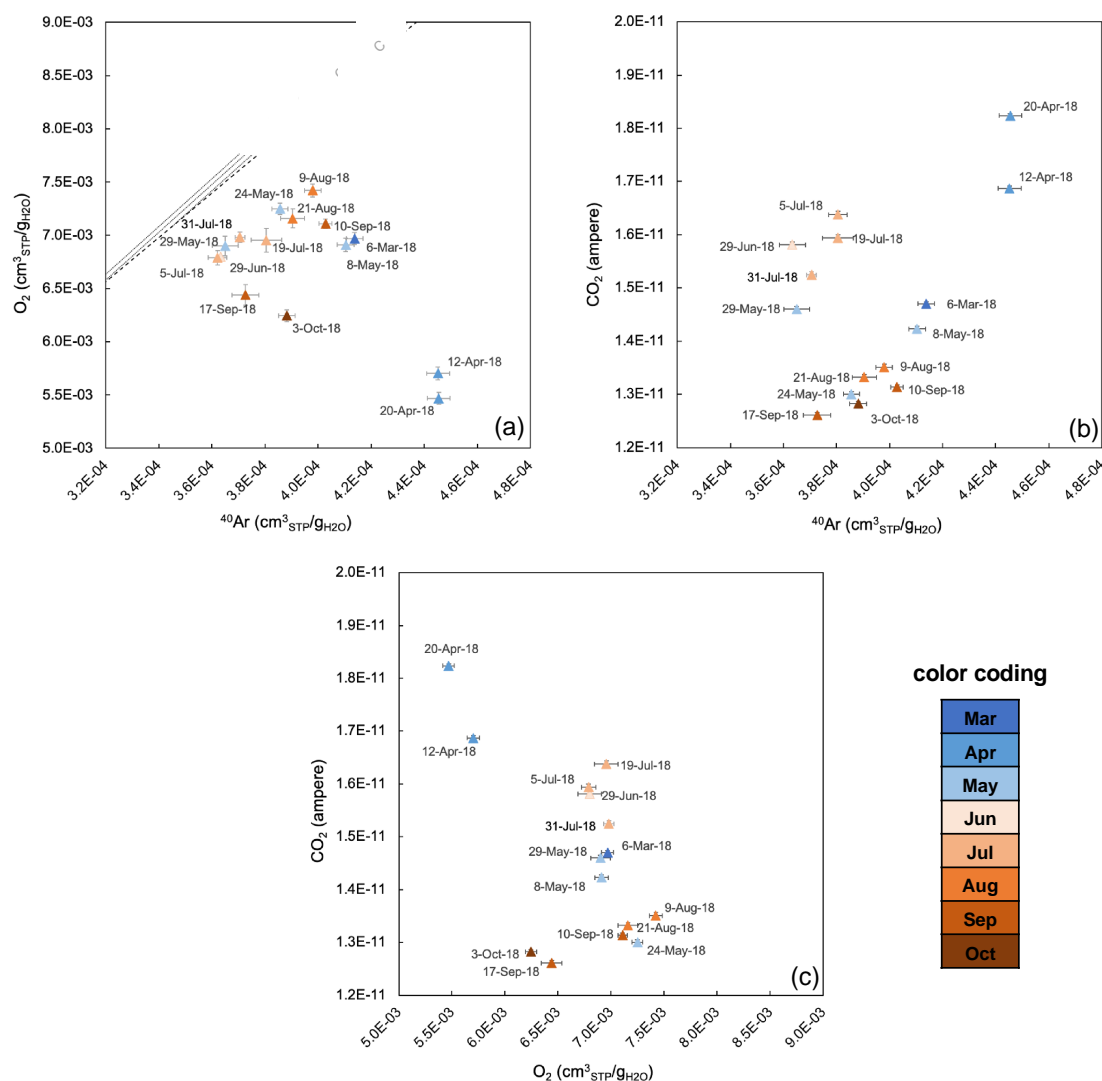
Figure 6: Bi-species plots of average concentrations of O_2 and ^{40}Ar and average ion current readings of CO_2 observed in the deep GW well (P7A.1b). Markers are color coded by sampling month and error bars represent 2-σ uncertainty intervals. The dashed line represents ASW between 0°C and 30°C. Dotted lines represent hypothetical additions of unfractionated excess air to ASW at different temperatures.

3.5 Noble gas recharge temperatures and excess air

The ratios of Ne/Ar and of $^4He/^{20}Ne$ determined from the high-resolution noble gas isotope analysis of the deep GW for the copper tube sample taken on 29-May-2018 were (5.64 ± 0.06)·10^{-4} and 0.243 ± 0.003, respectively, and correspond to ASW ratios between 0°C and 15°C. The elemental composition of any addition of EA must, therefore, be of nearly atmospheric composition, that is, unfractionated and the fractionation coefficient F can be set to 0. The measured $^{40}Ar/^{36}Ar$ ratio of the deep GW was 297.11 ± 0.82, which agrees with the atmospheric equilibrium ratio, as could be expected from the hydrology of the studied site. It can, therefore, be concluded that the observed ^{40}Ar in GW is of atmospheric origin. Similarly, based on the relatively short GW residence time of 3.9 years and the high ^3H activity (9.6 TU), it can be concluded that the observed excess in He is exclusively a result of the addition of EA. Therefore, ^{40}Ar and He are suitable for the quantification of T_R and A_e using the CE model with F set to 0 (i.e., the UA model). However, for improved uncertainty quantification, NGRT resulting from the UA model were compared to NGRT resulting from the CE model with F set

to 0.7, the upper limit of F still in agreement with the measured concentrations of ^{40}Ar and He. For P_R and S_R, the average values observed during the study period were used (i.e., 911 hPa and 0 g/kg).

NGRT and EA quantified with the UA model varied between 0.6 and 10.3°C and 0 and 1.8·10^{-3} cm$^3_{STP}$/g$_{H_2O}$, respectively (individual values are provided in **Supporting Information Table S2**). The average uncertainty of NGRT estimated with the UA model was 0.55°C. The average absolute difference between NGRT estimated with the UA model and NGRT estimated with the CE model and F=0.5 was 0.07°C and 0.2°C for F=0.7. The variation in NGRT arising from the uncertainty of F is thus substantially smaller than the average uncertainty of the estimated NGRT. Average daily NGRT and EA values are illustrated alongside hydraulic and meteorological observations in **Figure 3**. The seasonality that could be observed in the dissolved gas concentrations (see **Figures 5 and 6**) is also clearly visible in NGRT and EA (**Figure 3**). The lowest NGRT and the highest EA were observed approximately one month before the onset of snowmelt recharge, while during the spring snowmelt period, NGRT increased and EA decreased. NGRT rose earlier than the measured SW or GW temperatures during the snowmelt period and decreased earlier than air, SW or GW temperatures as summer progressed. The amplitude of NGRT was smaller than the amplitude of air or SW temperatures, but larger than the amplitude of deep and upstream GW temperatures. The amplitude of NGRT most closely mimics the amplitude of shallow GW temperatures. However, the fact that the lowest NGRT were observed about one month before the onset of the snowmelt period and that NGRT decreased earlier in the year compared to the shallow GW temperature indicates a significant temporal shift between recharge and the arrival of GW at the outlet of 7A.

4 Discussion

4.1 Snowmelt recharge analysis
The contribution of snowmelt to GW recharge was quantified using a residual water balance approach (**section 4.1.1**) and a two-component end-member mixing analysis (EMMA; Christophersen and Hooper (1992); Coplen et al. (2000)) based either on δ^2H and δ^{18}O (**section 4.1.2**) or NGRT (**section 4.1.3**). All results are summarized in **Table 2**. As the procedure for EMMA based on δ^{18}O is identical to that based on δ^2H, in **section 4.1.2** the procedure is only presented for δ^2H, and snowmelt recharge estimated with δ^{18}O is only provided in **Table 2**.

Table 2: Overview of the contribution of snowmelt to recharge.

Contribution of snowmelt to GW

Method	Snowmelt end-member	Fraction of total recharge	Temporal variation
Water balance	-	40 ± 20 %	-
δ^2H	snowfall	25 ± 20 %	-
	snowpack	23 ± 20 %	-
	stream water	58 ± 20 %	-
δ^{18}O	snowfall	31 ± 20 %	-
	snowpack	30 ± 20 %	-
	stream water	64 ± 20 %	-
NGRT	soil temperature	59 ± 20 %	95% (end of winter), 35% (summer)
	stream temperature	58 ± 20 %	100% (end of winter), 20% (summer)
	shallow GW temperature	47 ± 20 %	100% (end of winter), 0% (summer)

4.1.1 Estimation based on a residual water balance

Daily recharge was calculated with **Equation 1** and is shown in **Figure 3** (detailed data are provided as part of **Supporting Information Table S1**). According to the residual water balance approach, snowmelt recharge occurred from 25-Apr-2018 until 01-June-2018 and amounted to 336 mm, or 40% of the total recharge in 2018. Owing to the high-resolution measurement network, measurement uncertainties are only 5% for Q_{SW} and ET, 10% for P, and 15% for ΔS_{snow} (Isabelle et al., 2020a). Uncertainties for $Q_{baseflow}$ estimated with the digital recursive filter are 10% (Nathan & McMahon, 1990). The resulting uncertainty of snowmelt recharge is 20%.

4.1.2 Estimation based on stable water isotopes

The rain end-member is given by the mean δ^2H of rain (i.e., -69.0‰). The large temporal and spatial variations in the isotopic signal of snow (see **Figure 4**) make identifying the most representative end-member signal for snowmelt a difficult task prone to bias. To account for this, the sensitivity of snowmelt recharge to the choice of the snowmelt end-member definition was evaluated by testing three conceptually different definitions (see **Figure 4**): (i) The mean δ^2H of snowfall during winter (-127.9‰), (ii) the mean δ^2H of the snowpack during the onset of snowmelt (-133.9‰), and (iii) the mean δ^2H of in-stream SW during the peak of the spring snowmelt period (-94.8‰).

Based on these snowmelt end-member definitions, EMMA results in 25% snowmelt recharge using the mean δ^2H of snowfall, and in 23% snowmelt recharge using the mean δ^2H in the snowpack during the onset of snowmelt. In contrast to these low snowmelt recharge estimates, using the mean δ^2H of in-stream SW results in 58% snowmelt recharge. The analytical uncertainty of δ^2H (and $\delta^{18}O$) propagates to a theoretical uncertainty of only 2% for snowmelt recharge. However, the fact that the fraction of snowmelt recharge varies so strongly as a function of the snowmelt end-member definition provides clear evidence that snowmelt recharge estimated with stable water isotopes is strongly biased and that propagation of the analytical uncertainty is a purely theoretical procedure. With the variability in snowmelt recharge estimates resulting from different end-member assumptions being a more realistic estimate of the uncertainty of the approach, the actual uncertainty is likely on the order of 20%.

4.1.3 Estimation based on noble gas recharge temperatures

Identifying the most appropriate end-member signals for snowmelt and rain in an NGRT-based snowmelt recharge estimation is not straightforward. In principle, soil, shallow GW and in-stream SW temperatures all exhibit sufficiently large amplitudes to explain the observed variation in NGRT. As the most representative proxy is *a priori* unknown, the sensitivity of snowmelt recharge estimates to the end-member definition was evaluated by using all three aforementioned end-member definitions. Mean temperatures observed during the snowmelt period (23-Apr-2018 until 30-May-2018) were used to define the snowmelt end-member: (i) 0.6°C for soil, (ii) 2.1°C for in-stream SW, and (iii) 2.2°C for shallow GW. To define the rain end-member, mean temperatures during the snow-free summer period (1-June-2018 until 30-Sep-2018) were used: (i) 12.2°C for soil, (ii) 9.8°C for in-stream SW, and (iii) 8.1°C for shallow GW.

Using soil temperatures, the average contribution of snowmelt recharge was 59%, varying seasonally between 96% (20-Apr-2018) and 34% (29-Jun-2018). Using in-stream SW temperatures, the average contribution of snowmelt recharge was 58%, varying seasonally between 100% (20-Apr-2018) and 19% (29-Jun-2018). Using shallow GW temperatures, the average contribution of snowmelt recharge was 47%, varying seasonally between 100% (20-Apr-2018) and 0% (29-Jun-2018). Addressing both the propagated uncertainty for NGRT using

the UA model (i.e., 0.55°C) as well as the difference to the CE model with F set to 0.7 (i.e., 0.2°C), the uncertainty of NGRT for EMMA was assumed to be 1.0°C. The average uncertainty of end-member temperature definitions through direct temperature measurements was assumed to be 0.5°C. These uncertainties propagate to an average uncertainty of 20% for snowmelt recharge estimates. In contrast to the stable water isotopes-based approach, the variations in snowmelt recharge that result from different end-member definitions are well within the range of the theoretical uncertainty of the NGRT-based approach. Despite a similar apparent uncertainty as the stable water isotopes-based approach, the fact that snowmelt recharge estimates are much more consistent across three different end-member proxies demonstrates the robustness of NGRT-based snowmelt recharge estimation against potential bias originating from *a priori* unknown end-members.

4.2 Evidence for recharge through an extensive unsaturated zone

The observed depletion in dissolved O_2 and supersaturation in dissolved CO_2 is a common finding for GW and a result of the ubiquitous microbial respiration in the subsurface (Kipfer et al., 2002; Mächler et al., 2013a; Mächler et al., 2013b). While an accurate quantification of individual CO_2 concentrations was not possible (see **section 2.4.3**), an approximation using the average ampere signal of CO_2 (see **section 3.4**) indicates that average concentrations of CO_2 in the deep GW are on the order of $6.5 \cdot 10^{-3}$ cm^3_{STP}/g_{H_2O}. Comparing this approximate concentration of CO_2 to the average concentration of O_2 in the deep GW reveals that the sum of CO_2 and O_2 is significantly larger than the initial atmospheric input of O_2. The dissolved CO_2 can, therefore, not be explained by atmospheric input of CO_2 and aerobic respiration in GW alone and a significant amount of production of CO_2 must take place in the soil under continuous input of O_2 while a complete escape of CO_2 is inhibited. This indicates that the input of O_2 and, thus, the primary recharge pathway, is via an extensive unsaturated zone that allows CO_2 production and entrapment in pore water under simultaneous reoxygenation (see Mächler et al. (2013a)).

4.3 Evidence for biological N-fixation from dissolved gas measurements

Biological N-fixation by cyanobacteria-moss associations within the topsoil of boreal forests has been identified to contribute up to 50% of the nitrogen accumulated in boreal forest trees (DeLuca et al., 2002; Puri et al., 2020; Rousk et al., 2014; Sponseller et al., 2016). So far, however, the exact pathway of N_2 delivery for biological N-fixation has not been identified and a connection between soil water, GW, recharge and biological N-fixation has not previously been made. The observed depletion in dissolved N_2 in GW may provide the first direct evidence for infiltrating pore water and GW to be the primary pathway of N_2 delivery for biological N-fixation.

To rationalize this hypothesis, the annual N-removal from GW in the catchment was quantified by multiplying the observed mean N_2 deficit in GW by the amount of annual GW outflow from the catchment (i.e., direct GW outflow plus baseflow, as identified via the residual water balance) and subsequently compared to reported N-fixation rates for boreal forests. The annual GW outflow in 2018 was $6.2 \cdot 10^8$ L/year (see **Supporting Information Table S1**). As the GW was always in an oxic state (see **section 3.4**), significant production of N_2 in the subsurface via microbiologically-mediated denitrification can be ruled out (Firestone et al., 1980; Popp et al., 2020; Vogel et al., 1981) and the initial amount of N_2 dissolved in an infiltrating water parcel is given by **Equation 3**. The average N_2 deficit observed during the study period is thus given by the average difference between $C_{N_2,R}$ and the observed amount of N_2 and amounted to 0.47 mg/L (for individual data see **Supporting Information Table S2**). Considering the GW outflow of 2018 and the catchment area of 1.25 km^2, the N_2 deficit in GW leaving the catchment

in 2018 was 4.7 kg N/(ha·year). This value is in the range of the 0.1-7 kg N/(ha·year) reported for boreal systems (Lindo et al., 2013). As the observed deficit is at the upper end of the reported range of N-fixation rates, delivery via N_2 dissolved in infiltrating water appears to be the primary pathway for biological N-fixation in boreal systems.

4.4 Conceptual flow model of the studied boreal headwater catchment

The predominant flow and recharge pathways of the studied boreal headwater catchment are illustrated conceptually in **Figure 7**. According to the residual water balance approach for 2018, of the total inflow to the catchment via precipitation 60% were rainfall and 40% snowfall, which is in agreement with the observed long-term partitioning between rainfall and snowfall (see **section 2.1**). 30% of the total inflow left the catchment again as *ET* and sublimation and 65% as SW (see **section 2.1**). Assuming steady state, 5% of the total inflow thus left the catchment as GW. Snowmelt contributed approximately 50% to recharge (see **Table 2**), which is significantly more than the contribution of snowfall to precipitation. The ^{3}H/^{3}He-residence time analysis suggests a lag of 3.9 ± 0.9 years between recharge and GW flowing out of the catchment, whereas ^{222}Rn data imply the absence of water younger than two weeks. This is in agreement with the appearance of the lowest noble gas recharge temperatures in the deep GW, which appeared approximately one month before the onset of the snowmelt period. The observed amount of excess air in the deep and shallow GW can only be explained if the water table rises rapidly by at least 1 m during the snowmelt recharge pulse and thereby entraps air (Holocher et al., 2002; Kipfer et al., 2002; Klump et al., 2008). Thus, given the hydrogeology of the catchment, the upward hydraulic gradient at the outlet, the observed 3.5 m water table rise in the upstream during the snowmelt recharge pulse and the absence of a variation in stable isotopes (i.e., a completely damped signal) in the deep and shallow GW, recharge must primarily take place in the upstream sections of the alluvium. The semi-confining alluvial deposits located in the center of the catchment must, therefore, lead to focused recharge in the upstream of the alluvium and result in a strong upward gradient from deep to shallow GW at the catchment outlet. The strong upward gradient and lower hydraulic conductivity inhibit local recharge at the outlet and promote a substantial contribution of GW to SW via baseflow (~50%). This conceptual flow model agrees with the reactive gases O_2 and CO_2, which revealed that recharge primarily takes place through an unsaturated zone. By passing through an unsaturated zone, the loss of temporal information in stable water isotopes of GW can be explained: Infiltrated snowmelt and rain are first stored and mixed in the unsaturated zone prior to recharging the GW. The pre-mixing of waters in the unsaturated zone and the temporal lag between snowmelt and the arrival of snowmelt recharge at the outlet of a catchment is a common observation, and is further augmented in the presence of spatially-heterogeneous recharge patterns (Schilling et al., 2017b; Smith et al., 2014).
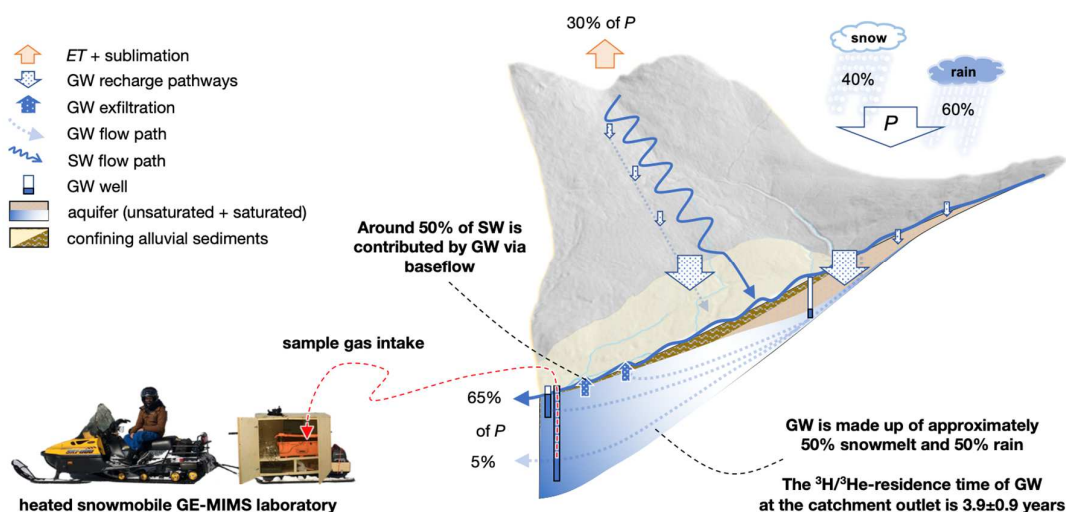
Figure 7: Conceptual model of the dominant flow and recharge pathways of the studied boreal headwater catchment. Illustrated alongside the main flow paths and water balance components for the year 2018 is the GE-MIMS heated snowmobile laboratory that was employed to measure dissolved gases on site.

4.5 Potential and limitations of dissolved gases for snowmelt recharge analysis

Dissolved noble gases are not governed by the same physical processes as stable water isotopes and as such, they provide different insights into snowmelt recharge dynamics. As they are part of the water molecule, stable water isotopes, on the one hand, are source-specific and the signal observed in GW derives directly from the signal in snowfall and rain (Beria et al., 2018; Jasechko, 2019). Dissolved noble gases, on the other hand, are not source-specific and the signal in GW acts as a record of the last time a parcel of water was in contact with the atmosphere and informs about the conditions encountered during recharge (Aeschbach-Hertig et al., 1999; Kipfer et al., 2002), thereby producing information that is complementary to stable water isotopes. While at the studied site, stable water isotopes had lost all temporal information on recharge due to mixing of infiltrated water in the unsaturated zone, dissolved noble gases still contained temporal information and indicated that a significant lag between recharge and the arrival of GW at the outlet of the catchment must exist (see **section 3.5**). Low NGRT and high EA were observed in winter before the spring snowmelt season, even though such a signal would be expected for concentrated infiltrating snowmelt. High NGRT and low EA, in contrast, were observed during and after the spring snowmelt period. The existence of long temporal lag was confirmed by the ^{3}H/^{3}He-residence time analysis. Note that in the hypothetical situation in which GW mixes so strongly that the seasonal signal in dissolved noble gases would become completely damped by the time GW reaches the outlet, NGRT could still be used to quantify the average contribution of snowmelt recharge even though the temporal information would be lost.

Due to the large spatial and temporal variability of the stable isotopic composition of water in snowfall, the snowpack, snowmelt and SW derived from snowmelt (see **Figure 4**), snowmelt recharge estimation with stable water isotopes is extremely sensitive to the choice of the snowmelt end-member proxy. As expected, using either δ^2H or δ^{18}O resulted in nearly identical estimates of snowmelt recharge (with δ^{18}O being systematically larger by 6-7%), but using different proxies resulted in a large spread ranging from 23% to 64% (see **Table 2**). In contrast to using stable water isotopes, NGRT produced snowmelt recharge estimates that were much

more consistent, ranging between 47% to 59% as a result of using different end-member proxies. Although the NGRT-based estimates are larger than the residual water balance-based estimate, they agree within one standard deviation and reflect the residual water balance-based estimate more closely than the stable water isotopes-based estimates (see **Table 2**). While, in principle, it would be possible to obtain an isotopic signal of snowmelt directly by capturing the melting snow underneath the snowpack, due the large variability of stable water isotopes in snowfall, the snowpack and snowmelt, an extremely elaborate sampling and technical infrastructure would be required to produce a truly representative signal for an entire catchment and snowmelt season (Bansah & Ali, 2017; Beria et al., 2018; Schmieder et al., 2016). Even in catchments as small as the one studied, the large variability in the original snowfall and snowpack isotopic composition (see **Figure 4**), in combination with complex winter hydrological processes (Parajuli et al., 2020a), makes obtaining a representative, direct signal of snowmelt a tantalizing, nearly impossible task, particularly as the impacts of winter hydrological processes (e.g., freezing/thawing, snow redistribution, rain-on-snow and melt-out) on the stable isotopic composition of water are not fully understood (Beria et al., 2018; Jasechko, 2019). While sophisticated upscaling or correction models may reduce the bias in snowmelt end-member definitions (e.g., Ala-Aho et al. (2017b)), bias cannot be prevented.

For the quantification of snowmelt recharge dynamics with dissolved gases, the variation in the recharge temperature must be larger than the uncertainty of the NGRT estimation. In snow-dominated catchments with relatively shallow water tables, significant seasonal water table fluctuations and impermeable bedrock that prevents inflow of GW from neighboring catchments, seasonal recharge temperature variations typically exceed the uncertainty of NGRT estimates, which makes dissolved noble gases useful tracers for the quantification of snowmelt recharge dynamics in these systems. However, in catchments with large elevation differences and/or more permeable bedrock (as for example encountered in basins with sedimentary or volcanic bedrock), deep water tables at higher elevations are common, and the temperature of infiltrating snowmelt and rain may approach the mean annual air temperature of the catchment before it reaches the water table (Doyle et al., 2015; Markovich et al., 2019), making seasonal recharge temperature signals invariable within the uncertainties of NGRT estimations. Consequently, dissolved gases are unsuitable as tracers of snowmelt recharge dynamics in these catchments. However, available data from high-elevation mountainous settings have also revealed that NGRT are either consistently 0-4°C below the mean annual air temperature (Manning, 2011; Manning & Solomon, 2003) or, where multiple measurements have been made at one site, showed considerable variation of 5°C or more (Masbruch et al., 2012; Singleton & Moran, 2010). These observations thus suggest that a snowmelt infiltration signal is indeed identifiable through NGRT and that a seasonal variation in NGRT is detectable not only in our catchment, but in high-elevation mountainous catchments as well.

While some observations suggest that rain and snow may be depleted in certain noble gases (Amalberti et al., 2018; Warrier et al., 2013), such a depletion has not been observed in snowmelt, and the assumption for snowmelt to be in equilibrium with atmospheric air appears to be valid for most catchments. However, while air in the snowpack and snowmelt can be expected to remain in equilibrium with atmospheric air (Severinghaus & Battle, 2006), glacial melt is typically depleted in the heavy noble gases (Grundl et al., 2013; Niu et al., 2017; Severinghaus & Battle, 2006), making a reliable estimation of snowmelt recharge with dissolved noble gases impossible in glaciated catchments without complementing stable water isotope measurements.

5 Conclusions

Stable water isotopes have long been the only suitable tracers for the quantification of snowmelt recharge, despite major limitations. For more than two decades, scientists and practitioners have called and searched systematically for alternative tracers capable of quantifying interactions between snowmelt, GW and SW. This study investigated whether dissolved gases (i.e., He, ^{40}Ar, ^{84}Kr, N_2, O_2 and CO_2) measured *in situ* in the field could be used as tracers for snowmelt-SW-GW dynamics and made steps towards bridging this gap.

At the investigated, snow-dominated boreal headwater catchment, dissolved noble gases showed to have a strong temperature dependence on recharge, making them highly suited for the quantification of snowmelt recharge dynamics. While stable water isotopes had lost all temporal information on recharge due to homogenization, that is, water mixing in the unsaturated zone, dissolved gases maintained a temporal signal and revealed a temporal lag of snowmelt recharge arrival at the catchment outlet compared to the actual snowmelt season. Not only did the dissolved noble gases allow recharge temperatures and the contribution of snowmelt to total recharge to be quantified, the combination of inert and reactive gases moreover made the case that the predominant recharge pathway is through a significant unsaturated zone. The fact that prior to reaching the GW, water remained a significant time in the unsaturated zone explained the homogenization observed in the stable water isotope signal. Due to pre-mixing in the unsaturated zone, the temporal information of the stable water isotopes at downstream GW wells was damped and masked.

The systematically depleted N_2 concentrations in the studied GW, furthermore, identified atmospheric N_2 as a primary source for biological N-fixation. The depletion in N_2 provided the first ever direct evidence that the principal pathway of delivery of atmospheric N_2 for biological N-fixation in boreal forests is via N_2 dissolved in soil and groundwater.

While stable water isotopes are more suited for the quantification of the water sources that contribute to GW, dissolved gases are more suited to inform about the timing and pathway of recharge. This difference arises from the different processes that govern stable water isotopes and dissolved gases: While stable water isotopes derive directly from the water source, dissolved gases mark the timing and pathway of recharge. As the timing and pathway are at least as important as the source of recharge for the development of sustainable management and a robust estimation of hydraulic properties, the combination of stable water isotope methods with advanced portable gas analysis opens a new and promising (experimental) avenue for the quantification of snowmelt-SW-GW dynamics.

Although dissolved noble gases are not as ubiquitously applicable as stable water isotopes for the estimation of snowmelt recharge, studies aimed at understanding snow-SW-GW dynamics should embrace the novel and portable dissolved gas measurement technology available through the GE-MIMS. The technology is highly versatile and could be employed directly on-site even under the harshest winter conditions by a simple construction of a heated snowmobile trailer laboratory. The simultaneous application of stable water isotopes and residence time analyses based on ^{222}Rn and ^{3}H/^{3}He together with on-site dissolved gas analysis revealed that the different methods are highly complementary and, thus, allow to tackle complex hydrological systems via a multi-tracer approach. A very promising future direction would be to combine such multi-tracer analyses of snowmelt-SW-GW dynamics with integrated surface-subsurface hydrological flow models (ISSHM) via tracer-aided model calibration, as predictions on the present and future behavior of snowmelt-SW-GW dynamics made with an ISSHM calibrated with tracer-based observations would allow the most robust management

strategies for water resources in snow-dominated regions to be devised (Brunner et al., 2017; Paniconi & Putti, 2015; Schilling et al., 2019a).

6 Acknowledgments

7 References

Aeschbach-Hertig, W., El-Gamal, H., Wieser, M., & Palcsu, L. (2008). Modeling excess air and degassing in groundwater by equilibrium partitioning with a gas phase. *Water Resour. Res., 44*(8). doi:10.1029/2007WR006454

Aeschbach-Hertig, W., Peeters, F., Beyerle, U., & Kipfer, R. (1999). Interpretation of dissolved atmospheric noble gases in natural waters. *Water Resour. Res., 35*(9), 2779-2792. doi:10.1029/1999WR900130

Aeschbach-Hertig, W., Peeters, F., Beyerle, U., & Kipfer, R. (2000). Palaeotemperature reconstruction from noble gases in ground water taking into account equilibration with entrapped air. *Nature, 405*(6790), 1040-1044. doi:10.1038/35016542

Aeschbach-Hertig, W., & Solomon, D. K. (2013). Noble gas thermometry in groundwater hydrology. In P. Burnard (Ed.), *Advances in Isotope Geochemistry*. Berlin Heidelberg, Germany: Springer.

Ala-Aho, P., Soulsby, C., Pokrovsky, O. S., Kirpotin, S. N., Karlsson, J., Serikova, S., . . . Tetzlaff, D. (2018). Using stable isotopes to assess surface water source dynamics and hydrological connectivity in a high-latitude wetland and permafrost influenced landscape. *J. Hydrol., 556*, 279-293. doi:10.1016/j.jhydrol.2017.11.024

Ala-Aho, P., Soulsby, C., Wang, H., & Tetzlaff, D. (2017a). Integrated surface-subsurface model to investigate the role of groundwater in headwater catchment runoff generation: A minimalist approach to parameterisation. *J. Hydrol., 547*, 664-677. doi:10.1016/j.jhydrol.2017.02.023

Ala-Aho, P., Tetzlaff, D., McNamara, J. P., Laudon, H., Kormos, P., & Soulsby, C. (2017b). Modeling the isotopic evolution of snowpack and snowmelt: Testing a spatially distributed parsimonious approach. *Water Resour. Res., 53*(7), 5812-5830. doi:10.1002/2017WR020650

Amalberti, J., Hall, C. M., & Castro, M. C. (2018). Noble gas signatures in snow. *Chem. Geol., 483*, 275-285. doi:10.1016/j.chemgeo.2018.02.022

Anderson, M. P., Woessner, W. W., & Hunt, R. J. (2015). *Applied groundwater modelling* (Second edition ed.). Oxford, United Kingdom: Academic Press.

Bansah, S., & Ali, G. (2017). Evaluating the effects of tracer choice and end-member definitions on hydrograph separation results across nested, seasonally cold watersheds. *Water Resour. Res., 53*(11), 8851-8871. doi:10.1002/2016WR020252

Barry, R., Plamondon, A. P., & Stein, J. (1988). Hydrologic soil properties and application of a soil moisture model in a balsam fir forest. *Can. J. For. Res., 18*, 427-434. doi:10.1139/x88-063

Beria, H., Larsen, J. R., Ceperley, N. C., Michelon, A., Vennemann, R., & Schaefli, B. (2018). Understanding snow hydrological processes through the lens of stable water isotopes. *WIREs Water, 5*(6). doi:10.1002/wat2.1311

Beyerle, U., Aeschbach-Hertig, W., Hofer, M., Imboden, D. M., Baur, H., & Kipfer, R. (1999). Infiltration of river water to a shallow aquifer investigated with $^3H/^3He$, noble gases and CFCs. *J. Hydrol., 220*, 169-185.

Böhlke, J. K. (2014). Variation in the terrestrial isotopic composition and atomic weight of argon (IUPAC Technical Report). *Pure Appl. Chem., 86*(9), 1421-1432. doi:10.1515/pac-2013-0918

Brennwald, M. S. (2014). *noblefit*. Zürich, Switzerland: Swiss Federal Institute of Aquatic Sciences (EAWAG). Retrieved from https://brennmat.github.io/noblefit/

Brennwald, M. S., Schmidt, M., Oser, J., & Kipfer, R. (2016). A portable and autonomous mass spectrometric system for on-site environmental gas analysis. *Environ. Sci. Technol., 50*, 13455-12463. doi:10.1021/acs.est.6b03669

Brunner, P., Therrien, R., Renard, P., Simmons, C. T., & Hendricks Franssen, H.-J. (2017). Advances in understanding river - groundwater interactions. *Rev. Geophys., 55*. doi:10.1002/2017RG000556

Carroll, R. W. H., Bearup, L. A., Brown, W., Dong, W., Bill, M., & Williams, K. H. (2018). Factors controlling seasonal groundwater and solute flux from snow-dominated basins. *Hydrol. Process., 32*, 2187-2202. doi:10.1002/hyp.13151

Cartwright, I., Cendón, D., Currell, M., & Meredith, K. (2017). A review of radioactive isotopes and other residence time tracers in understanding groundwater recharge: Possibilities, challenges, and limitations. *J. Hydrol., 555*, 797-811. doi:10.1016/j.jhydrol.2017.10.053

Cartwright, I., & Morgenstern, U. (2018). Using tritium and other geochemical tracers to address the "old water paradox" in headwater catchments. *J. Hydrol., 563*, 13-21. doi:10.1016/j.jhydrol.2018.05.060

Christophersen, N., & Hooper, R. P. (1992). Multivariate analysis of stream water chemical data: The use of principal components analysis for the end-member mixing problem. *Water Resour. Res., 28*(1), 99-107. doi:10.1029/91wr02518

Cook, P. G., & Herczeg, A. L. (2000). *Environmental tracers in subsurface hydrology*. New York: Springer.

Coplen, T. B., Herczeg, A. L., & Barnes, C. (2000). Isotope Engineering - Using stable isotopes of the water molecule to solve practical problems. In P. G. Cook & A. L. Herczeg (Eds.), *Environmental tracers in subsurface hydrology*. New York: Springer.

DeLuca, T. H., Zackarisson, O., Nilsson, M.-C., & Sellstedt, A. (2002). Quantifying nitrogen-fixation in feather moss carpets of boreal forests. *Nature, 419*, 917-920. doi:10.1038/nature01051

DeLuca, T. H., Zackrisson, O., Gundale, M. J., & Nilsson, M.-C. (2008). Ecosystem feedbacks and nitrogen fixation in boreal forests. *Science, 320*(5880), 1181-1181. doi:10.1126/science.1154836

DeWalle, D. R., & Rango, A. (2008). *Principles of snow hydrology*. Cambridge, UK: Cambridge University Press.

Doyle, J. M., Gleeson, T., Manning, A. H., & Mayer, K. U. (2015). Using noble gas tracers to constrain a groundwater flow model with recharge elevations: A novel approach for mountainous terrain. *Water Resour. Res., 51*(10), 8094-8113. doi:10.1002/2015WR017274

Earman, S., Campbell, A. R., Phillips, F. M., & Newman, B. D. (2006). Isotopic exchange between snow and atmospheric water vapor: Estimation of the snowmelt component of groundwater recharge in the southwestern United States. *J. Geophys. Res. Atmos., 111*(D9). doi:10.1029/2005JD006470

ECCC. (2013). Canadian climate normals 1981-2010. Retrieved 16.01.2019, from Environment and Climate Change Canada (ECCC)

ECCC. (2019). Foret Montmorency RCS - historic data search. from Environment and Climate Change Canada (ECCC) http://climat.meteo.gc.ca/historical_data/search_historic_data_f.html

Eckhardt, K. (2005). How to construct recursive digital filters for baseflow separation. *Hydrol. Process., 19*, 507-515. doi:10.1002/hyp.5675

Esri. (2019). *World Imagery Basemap*. Retrieved from: https://www.arcgis.com/home/item.html?id=10df2279f9684e4a9f6a7f08febac2a9

Firestone, M. K., Firestone, R. B., & Tiedje, J. M. (1980). Nitrous oxide from soil denitrification: Factors controlling its biological production. *Science, 208*(4445), 749-751. doi:10.1126/science.208.4445.749

Fuka, D. R., Walter, M. T., Archibald, J. A., Steenhuis, T. S., & Easton, Z. M. (2018). Package 'EcoHydRology' - A community modeling foundation for eco-hydrology (Version 0.4.12.1). CRAN.

Galewsky, J., Steen-Larsen, H. C., Field, R. D., Worden, J., Risi, C., & Schneider, M. (2016). Stable isotopes in atmospheric water vapor and applications to the hydrologic cycle. *Rev. Geophys., 54*(4), 809-865. doi:10.1002/2015RG000512

Gelhar, L. W., Welty, C., & Rehfeldt, K. R. (1992). A critical review of data on field-scale dispersion in aquifers. *Water Resour. Res., 28*(7), 1955-1974. doi:10.1029/92WR00607

Grundl, R., Magnusson, N., Brennwald, M. S., & Kipfer, R. (2013). Mechanisms of subglacial groundwater recharge as derived from noble gas,

14C, and stable isotopic data. *Earth Planet. Sci. Lett., 363-370*, 78-85. doi:10.1016/j.epsl.2013.03.012

Hadiwijaya, B., Pepin, S., Isabelle, P.-E., & Nadeau, D. F. (2020). The dynamics of transpiration to evapotranspiration ratio under wet and dry canopy conditions in a humid boreal forest. *Forest, 11*(2), 237. doi:10.3390/f11020237

Hayashi, M., & Farrow, C. R. (2014). Watershed-scale response of groundwater recharge to inter-annual and inter-decadal variability in precipitation (Alberta, Canada). *Hydrogeol. J., 22*(8), 1825-1839. doi:10.1007/s10040-014-1176-3

Healy, R. W., & Scanlon, B. (2010). *Estimating groundwater recharge*. Cambridge, UK: Cambridge University Press.

Heaton, T. H. E., & Vogel, J. C. (1981). "Excess Air" in groundwater. *J. Hydrol., 50*, 201-216. doi:10.1016/0022-1694(81)90070-6

Heilweil, V. M., Solomon, D. K., Perkins, K. S., & Ellett, K. M. (2004). Gas-partitioning tracer test to quantify trapped gas during recharge. *Ground Water, 42*, 589-600. doi:10.1111/j.1745-6584.2004.tb02627.x

Holocher, J., Matta, V., Aeschbach-Hertig, W., Beyerle, U., Hofer, M., Peeters, F., & Kipfer, R. (2001). Noble gas and major element constraints on the water dynamics in an alpine floodplain. *Ground Water, 39*(6), 841-852. doi:10.1111/j.1745-6584.2001.tb02472.x

Holocher, J., Peeters, F., Aeschbach-Hertig, W., Hofer, M., Brennwald, M. S., Kinzelbach, W., & Kipfer, R. (2002). Experimental investigations on the formation of excess air in

quasi-saturated porous media. *Geochim. Cosmochim. Acta, 66*(23), 4103-4117. doi:10.1016/S0016-7037(02)00992-4

Isabelle, P.-E., Nadeau, D. F., Anctil, F., Rousseau, A. N., Jutras, S., & Music, B. (2020a). Impacts of high precipitation on the energy and water budgets of a humid boreal forest. *Agric. For. Meteorol., 280*. doi:10.1016/j.agrformet.2019.107813

Isabelle, P.-E., Nadeau, D. F., Asselin, M.-H., Harvey, R., Musselman, K. N., Rousseau, A. N., & Anctil, F. (2018). Solar radiation transmittance of a boreal balsam fir canopy: Spatiotemporal variability and impacts on growing season hydrology. *Agric. For. Meterol., 263*, 1-14. doi:10.1016/j.agrformet.2018.07.022

Isabelle, P.-E., Nadeau, D. F., Perelet, A. O., Pardyjak, E. R., Rousseau, A. N., & Anctil, F. (2020b). Application and evaluation of a two-wavelength scintillometry system for operation in a complex shallow boreal-forested valley. *Boundary Layer Meteorol., 174*, 341-370. doi:10.1007/s10546-019-00488-7

Jasechko, S. (2019). Global isotope hydrogeology - Review. *Rev. Geophys.* doi:10.1029/2018RG000627

Jasechko, S., Wassenaar, L. I., & Mayer, B. (2017). Isotopic evidence for widespread cold-season-biased groundwater recharge and young streamflow across central Canada. *Hydrol. Process., 31*(12), 2196-2209. doi:10.1002/hyp.11175

Jung, M., & Aeschbach-Hertig, W. (2018). A new software tool for the analysis of noble gas data sets from (ground)water. *Environ. Model. Softw., 103*, 120-130. doi:10.1016/j.envsoft.2018.02.004

Kendall, C., & McDonnell, J. J. (1998). *Isotope tracers in catchment hydrology*. Netherlands: Elsevier.

Kinar, N. J., & Pomeroy, J. W. (2015). Measurement of the physical properties of the snowpack. *Rev. Geophys., 53*, 481-544. doi:10.1002/2015RG000481

Kipfer, R., Aeschbach-Hertig, W., Peeters, F., & Stute, M. (2002). Noble gases in lakes and ground waters. In D. Porcelli, C. Ballentine, & R. Wieler (Eds.), *Noble gases in geochemistry and cosmochemistry* (Vol. 47, pp. 615-700).

Klump, S., Cirpka, O. A., Surbeck, H., & Kipfer, R. (2008). Experimental and numerical studies on excess-air formation in quasi-saturated porous media. *Water Resour. Res., 44*(5). doi:10.1029/2007WR006280

Kormos, P. R., Marks, D., McNamara, J. P., Marshall, H. P., Winstral, A., & Flores, A. N. (2014). Snow distribution, melt and surface water inputs to the soil in the mountain rain–snow transition zone. *J. Hydrol., 519*, 190-204. doi:10.1016/j.jhydrol.2014.06.051

Kurtz, W., Lapin, A., Schilling, O. S., Tang, Q., Schiller, E., Braun, T., . . . Brunner, P. (2017). Integrating hydrological modelling, data assimilation and cloud computing for real-time management of water resources. *Environ. Model. Softw., 93*, 418-135. doi:10.1016/j.envsoft.2017.03.011

Kuypers, M. M. M., Marchant, H. K., & Kartal, B. (2018). The microbial nitrogen-cycling network. *Nat. Rev. Microbiol., 16*(5), 263-276. doi:10.1038/nrmicro.2018.9

Lafrenière, M. J., & Lamoureux, S. F. (2019). Effects of changing permafrost conditions on hydrological processes and fluvial fluxes. *Earth Sci. Rev., 191*, 212-223. doi:10.1016/j.earscirev.2019.02.018

Lavigne, M.-P. (2007). *Modélisation du régime hydrologique et de l'impact des coupes forestières sur l'écoulement du Ruisseau des Eaux-Volées à l'aide d'HYDROTEL.* (Master of Science), Institut national de la recherche scientifique (INRS). Retrieved from http://espace.inrs.ca/446/

Légaré-Couture, G., & Parent, M. (Cartographer). (2018). Carte de la géologie du quaternaire - Bassin versant du ruisseau des Eaux-Volées (BEREV), Forêt Montmorency. Échelle 1 : 10 000.

Li, D., Wrzesien, M. L., Durand, M., Adam, J., & Lettenmaier, D. P. (2017). How much runoff originates as snow in the western United States, and how will that change in the future? *Geophys. Res. Lett., 44*(12), 6163-6172. doi:10.1002/2017GL073551

Li, L., Maier, H. R., Partington, D., Lambert, M. F., & Simmons, C. T. (2014). Performance assessment and improvement of recursive digital baseflow filters for catchments with different physical characteristics and hydrological inputs. *Environ. Model. Softw., 54*, 39-52. doi:10.1016/j.envsoft.2013.12.011

Lindo, Z., Nilsson, M. C., & Gundale, M. J. (2013). Bryophyte-cyanobacteria associations as regulators of the northern latitude carbon balance in response to global change. Global Change Biology 19: 2022–2035. *Glob. Chang. Biol., 19*, 2022-2035. doi:10.1111/gcb.12175

Luke, S. H., Luckai, N. J., Burke, J. M., & Prepas, E. E. (2007). Riparian areas in the Canadian boreal forest and linkages with water quality in streams. *Environ. Rev., 15*, 79-97. doi:10.1139/a07-001

Lundberg, A., Ala-Aho, P., Eklo, O. M., Klöve, B., Kværner, J., & Stumpp, C. (2016). Snow and frost: implications for spatiotemporal infiltration patterns - a review. *Hydrol. Process., 30*, 1230-1250. doi:10.1002/hyp.10703

Lundquist, J. D. (2018). The value of snow. *Eos, 99*. doi:10.1029/2018EO109957

Lyne, V. D., & Hollick, M. (1979). *Stochastic time-variable rainfall-runoff modelling.* Paper presented at the Hydrology and Water Resources Symposium, Canberra.

Mächler, L., Brennwald, M. S., & Kipfer, R. (2012). Membrane inlet mass spectrometer for the quasi-continuous on-site analysis of dissolved gases in groundwater. *Environ. Sci. Technol., 46*, 8288-8296. doi:10.1021/es3004409

Mächler, L., Brennwald, M. S., & Kipfer, R. (2013a). Argon concentration time-series as a tool to study gas dynamics in the hyporheic zone. *Environ. Sci. Technol., 47*, 7060-7066. doi:10.1021/es305309b

Mächler, L., Brennwald, M. S., Tyroller, L., Livingstone, D. M., & Kipfer, R. (2014). Conquering the outdoors with on-site mass spectrometry. *CHIMIA, 68*(3), 155-159. doi:10.2533/chimia.2014.155

Mächler, L., Peter, S., Brennwald, M. S., & Kipfer, R. (2013b). Excess air formation as a mechanism for delivering oxygen to groundwater. *Water Resour. Res., 49*(10), 6847-6856. doi:10.1002/wrcr.20547

Manning, A. H. (2011). Mountain-block recharge, present and past, in the eastern Española Basin, New Mexico, USA. *Hydrogeol. J., 19*, 379-397. doi:10.1007/s10040-010-0696-8

Manning, A. H., & Caine, J. S. (2007). Groundwater noble gas, age, and temperature signatures in an Alpine watershed: Valuable tools in conceptual model development. *Water Resour. Res., 43*(4). doi:10.1029/2006WR005349

Manning, A. H., & Solomon, D. K. (2003). Using noble gases to investigate mountain-front recharge. *J. Hydrol., 275*, 194-207. doi:10.1016/S0022-1694(03)00043-X

Manning, A. H., & Solomon, D. K. (2005). An integrated environmental tracer approach to characterizing groundwater circulation in a mountain block. *Water Resour. Res., 41*(12). doi:10.1029/2005WR004178

Markovich, K. H., Manning, A. H., Condon, L. E., & McIntosh, J. (2019). Mountain-block recharge: A review of current understanding. *Water Resour. Res., 55*(11), 8278-8304. doi:10.1029/2019WR025676

Masbruch, M. D., Chapman, D. S., & Solomon, D. K. (2012). Air, ground, and groundwater recharge temperatures in an alpine setting, Brighton Basin, Utah. *Water Resour. Res., 48*(10), W10530. doi:10.1029/2012WR012100

Mattle, N., Kinzelbach, W., Beyerle, U., Huggenberger, P., & Loosli, H. H. (2001). Exploring an aquifer system by integrating hydraulic, hydrogeologic and environmental tracer data in a three-dimensional hydrodynamic transport model. *J. Hydrol., 242*(3-4), 183-196. doi:10.1016/S0022-1694(00)00394-2

Maxwell, R. M., Putti, M., Meyerhoff, S., Delfs, J.-O., Fergusson, I. M., Ivanov, V., . . . Sulis, M. (2014). Surface-subsurface model intercomparison: A first set of benchmark results to diagnose integrated hydrology and feedbacks. *Water Resour. Res., 50*(2), 1531-1549. doi:10.1002/2013WR013725

Mayer, A., Sültenfuß, J., Travi, Y., Rebeix, R., Purtschert, R., Claude, C., . . . Conchetto, E. (2014). A multi-tracer study of groundwater origin and transit-time in the aquifers of the Venice region (Italy). *Appl. Geochem., 50*, 177-198. doi:10.1016/j.apgeochem.2013.10.009

McDonnell, J. J., & Beven, K. (2014). Debates—The future of hydrological sciences: A (common) path forward? A call to action aimed at understanding velocities, celerities and residence time distributions of the headwater hydrograph. *Water Resour. Res., 50*(6), 5342-5350. doi:10.1002/2013WR015141

MELCC. (2019). Discharge data station 051004. Retrieved 20.05.2019, from Ministère du Développement durable, de l'Environnement et de la Lutte contre les Changements Climatiques Québec (MELCC)

Meriö, L.-J., Ala-Aho, P., Linjama, J., Hjort, J., Kløve, B., & Marttila, H. (2019). Snow to precipitation ratio controls catchment storage and summer flows in boreal headwater catchments. doi:10.1029/2018WR023031

Nathan, R. J., & McMahon, T. A. (1990). Evaluation of automated techniques for base flow and recession analyses. *Water Resour. Res., 26*(7), 1465-1473. doi:10.1029/WR026i007p01465

Niu, Y., Castro, M. C., Hall, C. M., Aciego, S. M., & Arendt, C. A. (2017). Characterizing glacial meltwater sources in the Athabasca Glacier, Canada, using noble gases as tracers. *Appl. Geochem., 76*, 136-147. doi:10.1016/j.apgeochem.2016.11.015

Panday, S., & Huyakorn, P. S. (2004). A fully coupled physically-based spatially-distributed model for evaluating surface/subsurface flow. *Adv. Water Resour., 27*, 361-382. doi:10.1016/j.advwatres.2004.02.016

Paniconi, C., & Putti, M. (2015). Physically based modeling in catchment hydrology at 50: Survey and outlook. *Water Resour. Res., 51*(9), 7090-7129. doi:10.1002/2015WR017780

Parajuli, A., Nadeau, D. F., Anctil, F., Parent, A.-C., Bouchard, B., Girard, M., & Jutras, S. (2020a). Exploring the spatiotemporal variability of the snow water equivalent in a small boreal forest catchment through observation and modelling. *Hydrol. Process., 34*(11), 2628-2644. doi:10.1002/hyp.13756

Parajuli, A., Nadeau, D. F., Anctil, F., Schilling, O. S., & Jutras, S. (2020b). Does data availability constrain temperature-index snow model? A case study in the humid boreal forest. *Water, 12*(8), 2284. doi:10.3390/w12082284

Partington, D., Brunner, P., Simmons, C. T., Werner, A. D., Therrien, R., Maier, H. R., & Dandy, G. C. (2012). Evaluation of outputs from automated baseflow separation methods against simulated baseflow from a physically based, surface water-groundwater flow model. *J. Hydrol., 458-459*, 28-39. doi:10.1016/j.jhydrol.2012.06.029

Peeters, F., Beyerle, U., Aeschbach-Hertig, W., Holocher, J., Brennwald, M. S., & Kipfer, R. (2002). Improving noble gas based paleoclimate reconstruction and groundwater dating using $^{20}Ne/^{22}Ne$ ratios. *Geochim. Cosmochim. Acta, 67*(4), 587-600. doi:10.1016/S0016-7037(02)00969-9

Popp, A. L., Manning, C. C., Brennwald, M. S., & Kipfer, R. (2020). A new in situ method for tracing denitrification in riparian groundwater. *Environ. Sci. Technol., 54*(3), 1562-1472. doi:10.1021/acs.est.9b05393

Puri, A., Padda, K. P., & Chanway, C. P. (2020). Can naturally-occurring endophytic nitrogen-fixing bacteria of hybrid white spruce sustain boreal forest tree growth on extremely nutrient-poor soils? *Soil Biol. Biochem., 140*, 1-11. doi:10.1016/j.soilbio.2019.107642

Purtschert, R. (2008). Timescales and tracers. In W. M. Edmunds & P. Shand (Eds.), *Natural Groundwater Quality* (pp. 91-108). Oxford, UK: Blackwell Publishing Ltd.

Risser, D. W., Gburek, W. J., & Folmar, G. J. (2009). Comparison of recharge estimates at a small watershed in east-central Pennsylvania, USA. *Hydrogeol. J., 17*, 287-298. doi:10.1007/s10040-008-0406-y

Rochette, F. J. (1971). *Hydrogeological study of ,Ruisseau des Eaux Volées' experimental basin.* (Master of Science), University of Western Ontario, London, Canada.

Rolston, D. E. (2005). Aeration. In D. Hillel (Ed.), *Encyclopedia of Soils in the Environment* (pp. 17-21). New York, NY: Academic Press.

Rousk, K., Jones, D. L., & DeLuca, T. H. (2014). Moss-nitrogen input to boreal forest soils: Tracking ^{15}N in a field experiment. *Soil Biol. Biochem., 72*, 100-104. doi:10.1016/j.soilbio.2014.01.031

Scanlon, B., Healy, R. W., & Cook, P. G. (2002). Choosing appropriate techniques for quantifying groundwater recharge. *Hydrogeol. J., 10*, 18-39. doi:10.1007/s10040-0010176-2

Schilling, O. S., Brennwald, M. S., Kipfer, R., & Therrien, R. (2018). Quantifying the contribution of snowmelt to groundwater recharge with portable mass spectrometry-based dissolved gas analysis. *Goldschmidt Abstracts, 2257.*

Schilling, O. S., Cook, P. G., & Brunner, P. (2019a). Beyond classical observations in hydrogeology: The advantages of including exchange flux, temperature, tracer concentration, residence time and soil moisture observations in groundwater model calibration. *Rev. Geophys., 57*. doi:10.1029/2018RG000619

Schilling, O. S., Gerber, C., Partington, D. J., Purtschert, R., Brennwald, M. S., Kipfer, R., . . . Brunner, P. (2017a). Advancing physically-based flow simulations of alluvial systems through observations of ^{222}Rn, ^{3}H/^{3}He, atmospheric noble gases and the novel ^{37}Ar tracer method. *Water Resour. Res., 53*(12), 10465-10490. doi:10.1002/2017WR020754

Schilling, O. S., Irvine, D. J., Hendricks Franssen, H.-J., & Brunner, P. (2017b). Estimating the spatial extent of unsaturated zones in heterogeneous river-aquifer systems. *Water Resour. Res., 53*(12), 10583-10602. doi:10.1002/2017WR020409

Schilling, O. S., Parajuli, A., Tremblay Otis, C., Müller, T. U., Antolinez Quijano, W., Tremblay, Y., . . . Therrien, R. (2020). *BEREV data 2017-2018.* Retrieved from: https://doi.org/10.4211/hs.650ba9303d5942c2b36fa5beafbf612a

Schilling, O. S., Park, Y.-J., Therrien, R., & Nagare, R. M. (2019b). Integrated surface and subsurface hydrological modeling with snowmelt and pore water freeze-thaw. *Groundwater, 57*(1), 63-74. doi:10.1111/gwat.12841

Schmieder, J., Hanzer, F., Marke, T., Garvelmann, J., Warscher, M., Kunstmann, H., & Strasser, U. (2016). The importance of snowmelt spatiotemporal variability forisotope-based hydrograph separation in a high-elevation catchment. *Hydrol. Earth Syst. Sci., 20*, 5015-5033. doi:10.5194/hess-20-5015-2016

Severinghaus, J. P., & Battle, M. O. (2006). Fractionation of gases in polar ice during bubble close-off: New constraints from firn air Ne, Kr and Xe observations. *Earth Planet. Sci. Lett., 244*, 474-500. doi:10.1016/j.epsl.2006.01.032

Shanafield, M., & Cook, P. G. (2014). Transmission losses, infiltration and groundwater recharge through ephemeral and intermittent streambeds: A review of applied methods. *J. Hydrol., 511*, 518-529. doi:10.1016/j.jhydrol.2014.01.068

Singleton, M. J., & Moran, J. E. (2010). Dissolved noble gas and isotopic tracers reveal vulnerability of groundwater in a small, high-elevation catchment to predicted climate changes. *Water Resour. Res., 46*(10). doi:10.1029/2009WR008718

Sklash, M. G., & Farvolden, R. N. (1979). The role of groundwater in storm runoff. *J. Hydrol., 43*, 45-65 doi:10.1016/S0167-5648(09)70009-7

Smith, R. S., Moore, R. D., Weiler, M., & Jost, G. (2014). Spatial controls on groundwater response dynamics in a snowmelt-dominated montane catchment. *Hydrol. Earth Syst. Sci., 18*(5), 1835–1856. doi:10.5194/hess-18-1835-2014

Sponseller, R. A., Gundale, M. J., Futter, M., Ring, A., Näsholm, T., & Laudon, H. (2016). Nitrogen dynamics in managed boreal forests: Recent advances and future research directions. *Ambio., 45*, S175-S187. doi:10.1007/s13280-015-0755-4

Sturm, M. (2015). White water: Fifty years of snow research in WRR and the outlook for the future. *Water Resour. Res., 51*(7), 4948-4965. doi:10.1002/2015WR017242

Sturm, M., Goldstein, M. A., & Parr, C. (2017). Water and life from snow: A trillion dollar science question. *Water Resour. Res., 53*(5), 3534-3544. doi:10.1002/2017WR020840

Sturm, M., Taras, B., Liston, G. E., Derksen, C., Jonas, T., & Lea, J. (2010). Estimating snow water equivalent using snow depth data and climate classes. *J. Hydrometeorol., 11*, 1380-1394. doi:10.1175/2010JHM1202.1

Tetzlaff, D., Buttle, J., Carey, S. K., McGuire, K., Laudon, H., & Soulsby, C. (2014). Tracer-based assessment of flow paths, storage and runoff generation in northern catchments: a review. *Hydrol. Process., 29*, 3475-3490. doi:10.1002/ hyp.10412

Tomonaga, Y., Giroud, N., Brennwald, M. S., Horstmann, E., Diomidis, N., Kipfer, R., & Werisin, P. (2019). On-line monitoring of the gas composition in the full-scale emplacement experiment at Mont Terri (Switzerland). *Appl. Geochem., 100*, 234-243. doi:10.1016/j.apgeochem.2018.11.015

Tremblay Otis, C. (2018). *Estimation de la recharge à l'aide de différentes méthodes dans un sous-bassin au Québec.* (Master of Science), Université de Neuchâtel, Neuchâtel, Switzerland.

Tremblay, Y., Rousseau, A. N., Plamondon, A. P., Lévesque, D., & Jutras, S. (2008). Rainfall peak flow response to clearcutting 50% of three small watersheds in a boreal forest, Montmorency Forest, Québec. *J. Hydrol., 352*, 67-76. doi:10.1016/j.jhydrol.2007.12.028

Tremblay, Y., Rousseau, A. N., Plamondon, A. P., Lévesque, D., & Prévost, M. (2009). Changes in stream water quality due to logging of the boreal forest in the Montmorency Forest, Québec. *Hydrol. Process., 23*, 764-776. doi:10.1002/hyp.7175

Vaikmäe, R., Vallner, L., Loosli, H. H., Blaser, P. C., & Juillard-Tardent, M. (2001). Palaeogroundwater of glacial origin in the Cambrian-Vendian aquifer of northern Estonia. In E. W.M. & C. J. Milne (Eds.), *Palaeowaters in Coastal Europe: evolution of groundwater since the late Pleistocene* (Vol. 189, pp. 17-22). London: Geological Society.

Visser, A., Thaw, M., Deinhart, A., Bibby, R., Safeeq, M., Conklin, M., . . . Van der Helde, Y. (2019). Cosmogenic isotopes unravel the hydrochronology and water storage dynamics of the Southern Sierra critical zone. *Water Resour. Res., 55*(2), 1429-1450. doi:10.1029/2018WR023665

Vogel, J. C., Talma, A. S., & Heaton, T. H. E. (1981). Gaseous nitrogen as evidence for denitrification in groundwater. *J. Hydrol., 50*, 191-200. doi:10.1016/0022-1694(81)90069-X

Walvoord, M. A., & Kurylyk, B. L. (2016). Hydrologic impacts of thawing permafrost-A review. *Vadose Zone J., 15*(6). doi:10.2136/vzj2016.01.0010

Warrier, R. B., Castro, M. C., Hall, C. M., & Lohmann, K. C. (2013). Noble gas composition in rainwater and associated weather patterns. *Geophys. Res. Lett., 40*, 3248-3252. doi:10.1002/grl.50610

Weber, U. W., Cook, P. G., Brennwald, M. S., Kipfer, R., & Stieglitz, T. C. (2018). A novel approach to quantify air-water gas exchange in shallow surface waters using high-resolution time series of dissolved atmospheric gases. *Environ. Sci. Technol.* doi:10.1021/acs.est.8b05318

White, W. M. (2015). *Isotope geochemistry*. Hoboken, NJ: John Wiley and Sons Ltd.

Young, N. L., Lemieux, J. M., Delottier, H., Fortier, R., & Fortier, P. (2020). A conceptual model for anticipating the impact of landscape evolution on groundwater recharge in degrading permafrost environments. *Geophys. Res. Lett., 47*(11). doi:10.1029/2020GL087695